photonics

MDPI

Review

Optical Fiber Biosensors for Protein Detection: A Review

Shuhan Lyu [1,†], Zheyu Wu [2,*,†], Xinghua Shi [2] and Qian Wu [3]

[1] West Nottingham Academy, 1079 Firetower Road, Colora, MD 21917, USA
[2] Theory Laboratory, The National Center for Nanoscience and Technology, Beijing 100190, China
[3] Department of Mechanical and Aerospace Engineering, University of Missouri, 416 South 6th, Columbia, MI 65211, USA
* Correspondence: wuzy@nanoctr.cn; Tel.: +86-18702688012
† These authors contributed equally to this work.

Abstract: Proteins play an important role in organisms. The fast and high-accuracy detection of proteins is demanded in various fields, such as healthcare, food safty, and biosecurity, especially in the background of the globally raging severe acute respiratory syndrome coronavirus 2 (SARS-CoV-2). Optical fiber sensors have great potential for protein detection due to the excellent characteristics of high sensitivity, miniaturization, and capability for remote monitoring. Over the past decades, a large number of structures have been investigated and proposed. This paper begins with an overview of different fiber sensing structures for protein detection according to the fundamental sensing mechanisms. The overview is classified into four sections, including intensity-modulation, phase-modulation, scattering, and fluorescence. In each section, we reviewed the recent advances of fiber protein sensors and compared their performance, such as sensitivity and limit of detection. And then we analyzed the advantages and disadvantages of the four kinds of biosensors. Finally, the paper concludes with the challenges faced and possible future development of optical fiber protein biosensors for further study.

Keywords: biosensor; optical fiber; protein detection

Citation: Lyu, S.; Wu, Z.; Shi, X.; Wu, Q. Optical Fiber Biosensors for Protein Detection: A Review. *Photonics* **2022**, *9*, 987. https://doi.org/10.3390/photonics9120987

Received: 30 November 2022
Accepted: 12 December 2022
Published: 15 December 2022

1. Introduction

Proteins are essential parts of organisms and participate in virtually every process within cells that perform a vast array of functions within organisms, including catalysing metabolic reactions, DNA replication, responding to stimuli, providing structure to cells and organisms, and transporting molecules from one location to another. For example, enzymes that catalyze biochemical reactions have the effect of promoting metabolism. Membrane proteins play a special role in terms of structure and function [1]. The rapid and low-cost detection and identification of proteins is in great demand in biomedicine and the food industry. In recent decades, the demand for reliable and accurate sensing has fuelled the development of various protein detection methods, with each having several advantages and disadvantages. For instance, immunoblotting (or Western blotting) is a highly sensitive and specific assay method that works by exploiting the specificity inherent in antigen–antibody recognition [2]. However, it has a high cost and precise technical requirements. Immunohistochemistry is usually used to qualitatively analyze the expression of some proteins, while the method may present significant bias and has low sensitivity and specificity [3]. An enzyme-linked immunosorbent assay is a powerful tool for highly sensitive protein detection, but its disadvantages include low specificity, considerably long turn-around time, and a complicated labelling process [4]. Therefore, there is an urgent need to develop a fast, accurate, and cost-effective protein detection method for biomedical research.

Optical fiber sensors have acquired paramount importance in fields including environmental monitoring [5], medicine analysis [6], clinical diagnostics [7], and biochemical

detection [8] due to their compact size, high stability and robustness, immunity to electromagnetic interference, and remote operation potential. In parallel with the recent development of novel fiber-optic structures and materials sciences, the impressive performances of on-chip nano-photonic biosensors have been combined with those novel optical fibers, resulting in a complete research field called "Lab-on-Fiber" [9]. Optical fiber biosensors have had extraordinary growth in distinguishing biomolecules, such as proteins, DNA sequences [10], glucoses [11], and hormones [12], with high sensitivity and selectivity. Detection technology based on protein reaction is the most popular in biosensors due to its use in health monitoring [13], disease diagnosis [14], food safety [15], and biosecurity [16]. Over decades of research and development, optical fiber biosensors have proven to be a fast and reliable method for the detection of protein reaction kinetics.

Among optical fiber biosensors, two commonly used techniques are label and label-free techniques. The label technique is typically a sandwich structure. Most of the applications are combined with the fluorescence technique, which requires the fluorescently labelled antibody that can specifically bind to the target antigen. This can effectively reduce the interference of signals from non-specific binding of other interfering proteins, thereby drastically reducing the selectivity of the immunosensors. However, there are still some potential issues including time-consuming procedures, possible human error, mechanical damage, and risks of contamination [17]. The label-free technique is based on the modulation of the transmitting optical signals by the refractive index (RI) variations caused by bio-recognition events at the fiber sensor surface [18]. It has acquired paramount importance in immunosensors because of the advantages of being low cost, easy to perform, and free of the laborious labelling process. Moreover, the technique also provides the ability for the real-time monitoring of biochemical reactions [19,20].

As shown in Figure 1, there are three main steps in the fabrication of optical fiber biosensors, including the sensitization of the optical fiber and the modification of the receptor. Since most of the light is usually confined in the core of the fiber, it is crucial to modify the fiber structure for enhancing the interaction between light and the surrounding environment in the sensing area [21,22]. It has been proven that the sensitivity of indirect immobilization is higher than that of direct immobilization [14]. Various kinds of materials have been employed to modify the fiber surface. These materials either enhance the signal response affected by the biomedical reaction or increase the binding efficiency of the receptor. Subsequently, biomolecule receptors are immobilized on the functional materials. Finally, when the analytes bind with the receptors on the fiber surface, its biomedical reaction modifies the transmitted or reflected light signals in the optical fiber, which can be detected by optical interrogation. To date, the biosensors can sense protein molecules down to the fM level [23] with the support of various modification process.

Although recent years have witnessed fast development in optical fiber-based biosensors for protein recognition, a comprehensive and updated review of the biosensor has not appeared yet. This paper begins with an overview of different fiber sensing structures for protein detection according to the work mechanisms. This is followed by a comparison of the advantages and disadvantages of the four kinds of biosensors. Finally, this paper includes the outlook and discusses the challenges and opportunities for future development.

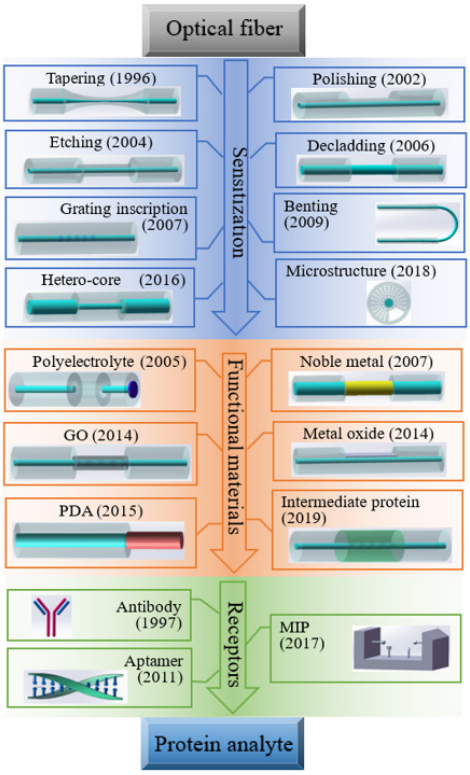

Figure 1. Schematic diagram of the fabrication of optical fiber biosensors for protein detection.

2. Protein Biosensors Based on Sensing Mechanisms and Recent Advances

The functional modification of optical fibers is a very important process. A biological receptor can be directly modified on the sensing region by the salinization process [24]. However, it has been proven that the sensitivity of indirect immobilization is higher than that of direct immobilization [14]. Various materials have been employed to modify the fiber surface, as shown in Figure 1. Noble metal nanofilms [25] and metal oxides [26] are usually used to couple the evanescent wave in order to modulate the transmission spectrum. Polydopamine (PDA) coating is an easy and versatile modification method [27]. Polyelectrolytes are usually deposited on the fiber surface using the layer-by-layer electrostatic self-assembly (LBL-ESA) technique, providing a spongy surface that contributes to preserving the bio-active ability of proteins and increasing the binding capacity of the absorbed bioreceptor [28,29]. Graphene oxide (GO) possesses excellent capabilities in biocompatibility, solubility, and selectivity [30], which can improve the biomolecule modification density, thereby increasing the sensitivity [31,32]. Some intermediate protein materials, such as protein A and protein G, have a high affinity with the crystallizable fragment region of the antibody molecule, extending the binding sites of the antigen-binding fragment region outward [33]. These materials either enhance the signal response affected by the biomedical reaction or increase the binding efficiency of the receptor.

To date, broad-spectrum biomolecule receptors have been utilized for protein recognition, including antibodies [34], aptamers [35], and molecularly imprinted polymers (MIPs) [36]. Antibodies are large and Y-shaped proteins, which can specifically recognize a unique antigen [37]. Aptamers are single-stranded oligonucleotide (DNA or RNA) or peptide molecules that bind to a specific target molecule, which are selected in vitro [38]. Compared to antibodies, they are more stable, flexible, mass-produced, and easy to modify [39,40]. MIPs are tailor-made chemical receptors obtained by the polymerization of functional monomers and crosslinker molecules in the presence of a template, which can recognize and bind target molecules with a high affinity and selectivity [41,42]. As compared with antibodies, they are easier to prepare, more cost efficient, and more stable [43]. In addition, there are some special bioconjugate pairs such as streptavidin–biotin [44].

Streptavidin (SV) has very high affinity for biotin, since it possesses one of the strongest noncovalent interactions in nature. Therefore, they are often used as demonstration models in biosensing.

Despite the diverse protein biosensors, the most widely used mechanism is based on the RI changes of the surrounding medium caused by protein recognition on the optical fiber surfaces. This is mainly due to the mature and highly sensitive refractive-index-sensing technology that relies on a variety of optical fiber structures [45–48]. According to the sensing mechanism, the modulations of transmitted light can also be roughly classified as intensity-modulation and phase-modulation.

2.1. Intensity-Based Fiber Biosensors

An evanescent wave is a rapid attenuation of electromagnetic waves concentrating near the core/cladding interface that occurs when the optical signals are transmitted in the optical fiber. Although an evanescent wave cannot propagate along optical fibers, it can exchange energy with the core mode and environmental materials. The evanescent wave absorption (EWA) characteristics of the materials deposited on the optical fiber can be used to achieve the selective absorption of a specific wavelength or spectral range [49]. When a broadband white-light source is injected into the optical fiber, most of the energy of a specific wavelength is absorbed by the coated materials, which sharply reduces the energy of the transmitted light. For absorption-based biosensors, the transmitted output light intensity, I_{out}, in optical fibers can be described by Beer–Lamber's law [50]:

$$I_{out} = I_{in}e^{-\alpha L} \quad (1)$$

where I_{in} is the input light intensity, L is the interaction length, and α is the attenuation coefficient, which relates to the fraction of light in the evanescent domain, molecular absorptivity, and its concentration. Then, by monitoring the intensity of this particular absorption dip, the selective detection of the target analyte can be achieved. The typical structures of EWA-based fiber biosensors are shown in Figure 2a–c.

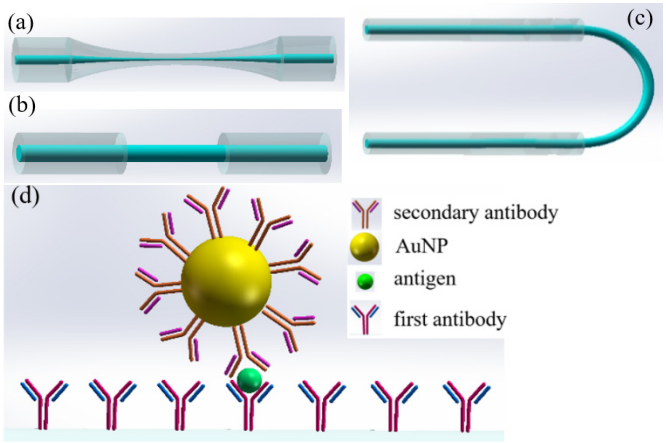

Figure 2. The schematic diagram of (**a**) microfiber, (**b**) unclad fiber, (**c**) U-bent unclad fiber, and (**d**) gold-linked sandwich immunoassay.

Proteins exhibit significant absorption of light at wavelengths of 280 nm and 260 nm, which are in the ultraviolet region. Sai et al. took advantage of that fact, developing a fiber-optic biosensor based on EWA at 280 nm to detect goat anti-human immunoglobulin G (GaHIgG) with a limit of detection (LoD) of 0.1 μg/mL [51]. However, the absorption sensitivity of the protein itself is low. In 2007, Leung et al. reported the use of a laser of 1550 nm and an antibody-modified tapered fiber-optic biosensor to monitor the attachment of bovine serum albumin (BSA) down to 10 fg/mL [52]. Although BSA was non-absorbing at 1550 nm, the absorption of the proteins to the tapered fiber leads to the change in RI. In 2018, Petropoulou et al. used a synthesis of novel amphiphilic block copolymers forming

a stable polymeric film on the optical fiber [53], which can absorb negatively charged proteins, such as BSA.

The more popular method is utilizing the extinction property of gold nanoparticles (AuNPs), which selectively absorb evanescent waves when they approach the fiber surface. The strong absorption of evanescent waves can be achieved using AuNPs as amplification markers combined with sensitized fiber platforms, and AuNPs are attached to the fiber sensing region via a sandwich structure as shown in Figure 2d. In 2014, Li et al. reported an optical microfiber (MF) using AuNPs as an amplification label for the detection of alphafetoprotein (AFP) with a LoD of 0.2 ng/mL [54]. In 2016, Bandaru et al. demonstrated a U-bent unclad fiber for human IgG (HIgG) detection with a LoD of 0.3 ng/mL [55]. Later, they reduced the LoD to 1 fg/mL with the silver enhancement of AuNP labels [56]. In 2020, Chiang et al. fabricated an unclad fiber for procalcitonin (PCT) detection providing a LoD of 95 fg/mL [57]. In 2021, Divagar et al. used a U-bent unclad fiber to detect severe acute respiratory syndrome coronavirus 2 (SARS-CoV-2) nucleocapsid protein (N-protein) [58]. Compared to the EWA-based label-free biosensors, the nanogold-linked immunosorbent assay method has higher sensitivity and better specificity.

Due to the small penetration depth of the evanescent waves, EWA-based fiber-optic sensors usually need to reduce the fiber diameter due to the requirement for a sufficient intensity of evanescent waves, which also increases the fragility of the optical fibers. In 2021, Xu et al. demonstrated an intensity-modulated all-fiber optofluidic biosensor based on Fresnel reflection [59]. As shown in Figure 3a,b, the biosensor consists of a single-multimode fiber coupler, multimode fiber (MMF) probe, and an optofluidic cell. When the incident light coupled into the fiber probe core, a fraction of the light was reflected on the end surface of the fiber probe according to the Snell–Descartes laws, then coupled back into the coupler sensor. On one hand, since the entire system is composed of non-bulk optical components, strict optical alignment is not required. On the other hand, the use of MMFs with a larger surface enhances the interaction between light and the analyte in the sensing interface. Thus, this biosensor has good light transmission efficiency and stability. With the help of this structure, they detected a SARS-CoV-2 spike protein receptor-binding domain (S-RBD) with a LoD of 0.005 ng/mL. Some important intensity-based fiber biosensors for protein dection are summerized in Table 1.

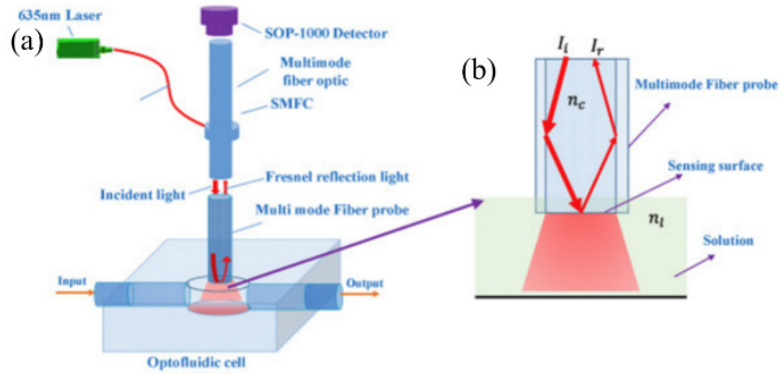

Figure 3. The schematic diagram of (**a**) the optofluidic biosensor based on Fresnel reflection and (**b**) the fiber probe immersed in liquid. Reprinted with permission from [59].

2.2. Phase Shift-Based Fiber Biosensors

The biosensors based on EWA might introduce a large insertion loss, due to the evanescent wave easily spreading into the measured solution. Optical fiber phased-modulated biosensors detect the surrounding protein molecules by measuring the cumulative optical phase variation of the light waves in the fibers caused by the biomedical reaction on the optical fiber surface during the light–matter interaction. The phase changes in the optical fiber usually result in the wavelength variation of the transmission spectra, which can be read out with the electromagnetic resonance, interferometers, and fiber gratings.

Table 1. Intensity-based fiber biosensors for protein detection.

Fiber Sensor Configuration	Detection Target	Functionalization Method	Sensitivity	Limit of Detection	Ref
Unclad Fiber	GaHIgG	Antigen	-	0.1 μg/mL	[51]
Tapered fiber	BSA	Antibody	-	~10 fg/mL	[52]
Unclad fiber	BSA	Amphiphilic block copolymers	-	~0.025% *w*/*v*	[53]
Tapered fiber	AFP	AuNPs absorption + antibody	-	0.2 ng/mL	[54]
U-bent unclad fiber	HIgG	AuNPs absorption + antibody	0.019 A_{530nm} /log (fg/mL)	0.3 ng/mL	[55]
U-bent unclad fiber	HIgG	Silver enhanced AuNPs absorption + antibody	0.281 A_{530nm} /log (fg/mL)	1 fg/mL	[56]
Unclad fiber	PCT	AuNPs absorption + antibody	-	95 fg/mL	[57]
U-bent unclad fiber	SARS-CoV-2 N-protein	AuNPs absorption + antibody	-	~2.5 ng/mL	[58]
Optofluidic SMFC	S-RBD	Antigen	-	0.005 ng/mL	[59]

2.2.1. Electromagnetic Resonance-Based Fiber Biosensors

Under the excitation of waveguide light, the metal or semiconductor nano-film deposited on the optical fibers generates and characterizes electromagnetic resonance (EMR). According the permittivity ($\varepsilon = \varepsilon' + j\varepsilon''$) or refractive index ($N = n + jk$) of the thin-films, where ε' and ε'' are the real and imaginary parts of the permittivity, n and k are the real and imaginary parts of the refractive index, respectively, and the EMR can be divided into: surface plasmon and resonance (SPR) and lossy mode resonance (LMR).

SPR Sensors

SPR is described as a surface electromagnetic wave stimulated by the excitation of surface plasmon polaritons, which are generated by the resonance of the evanescence wave and the surface plasmon wave on the surface between the optical fiber and metal thin-film [60]. Not only must the real part of the metal thin-film permittivity be negative and higher than the imaginary part, the permittivity of the material deposited also needs to be lower than that of the thin film [61]. Gold films are widely deposited on optical fibers by sputtering and thermal evaporation, due to gold's good resistance to oxidation and corrosion in different circumstances [62].

A wide variety of structures have been used for SPR-based fiber biosensors, including tapered fibers [36,63], unclad fibers [36], D-shaped fibers [16,64], U-bent fibers [65], tilted fiber Bragg gratings [33], and long period gratings [66], as shown in Figure 4a–f. For protein detection, it is of significance to immobilize the biomolecule receptors on the metal thin-film well. Bioactive molecules are generally immobilized on the surface of the golden film with the help of sulfhydryl (-SH). Since the strength of the Au-S bond is higher than that of the S-H bond, the biomolecules are easy to fix on the gold film surface with the formation of the Au-S bonds [67]. Moreover, Briand demonstrated that the co-adsorption of different thiols improves the stability and the molecular recognition properties of immobilized proteins due to reduced steric hindrance [68,69]. However, protein molecules are large, with complex structures, and do not necessarily have sulfhydryl. In order to solve this, the intermediate protein materials, such as protein A [70] and protein G [71], are used to immobilize the protein by linking the Au film and proteins. Wong et al. demonstrated a photonic crystal fiber SPR biosensor based on protein G immobilization to monitor the binding kinetics of the IgG and anti-IgG with a LoD of 0.267 mg/L [71]. The protein G could guide the bound antibody to a proper orientation on the surface. In addition, Shi et al. showed a surface functionalization method for the self-polymerization of PDA, which is simpler and quicker [27].

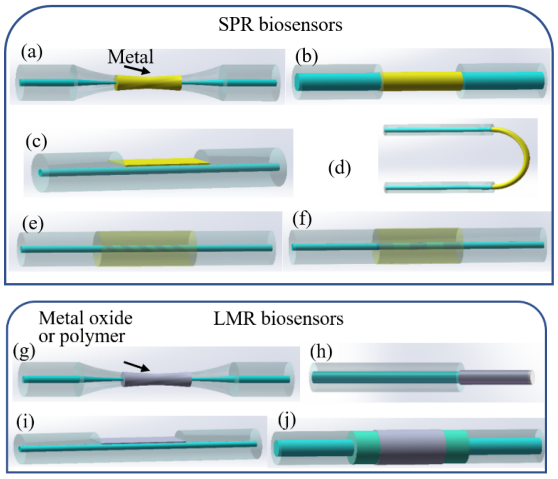

Figure 4. The schematic diagrams of SPR biosensors based on (**a**) MF, (**b**) unclad fiber, (**c**) D-shaped fiber, (**d**) U-bent fiber, (**e**) tilted fiber Bragg grating, and (**f**) long period grating and LMR biosensors based on (**g**) MF, (**h**) reflective unclad MMF, (**i**) D-shaped fiber, and (**j**) multimode-coreless-multimode (MCM) fiber structure.

Gold film is generally preferred because of its excellent antioxidant and corrosion resistance compared to other metals. However, gold film suffers from inefficient biomolecule immobilization efficiency [62]. In addition to gold, silver also often performs as the material for the metal film of SPR biosensors. Although silver has quite good sensitivity and a sharp SPR dip, it is easy to oxidize and form thin-film agglomerates [72]. SPR sensors based on GO-coated silver thin films can effectively prevent the oxidation of the silver film due to GO stopping the oxygen molecules from passing through the silver thin film [73]. Wang et al. demonstrated a GO/silver-coated polymer cladding silica (PCS) fiber for HIgG detection with a high sensitivity of 0.4985 nm/(μg/mL) and a low LoD of 0.04 μg/mL [74]. Furthermore, the sensitivity of the SPR fiber sensors incorporated with GO layers can be greatly enhanced compared to one of the conventional SPR fiber sensors. Owed to its large surface-to-volume ratio and good biocompatibility, GO provides the highest extraction efficiency of biomolecules per unit area [75].

In 2018, Wang et al. explored an optical fiber SPR biosensor based on GO and staphylococcal protein A (SPA) co-modified tilted fiber Bragg grating [33]. GO coating makes more antibodies attach to the sensor surface. Second, SPA binds to the antibodies directionally, improving the antigen–antibody binding efficiency. The co-modified biosensor shows high performance in the detection of HIgG with a sensitivity and LoD of 0.096 dB/(μg/mL) and 0.5 μg/mL, respectively. Recently, optical fiber biosensors based on localized surface plasmon resonance (LSPR) have attracted increasing attention; this is a kind of SPR phenomenon generated from metallic nanoparticles rather than bulk metal [76]. The size of these metallic nanoparticles is usually on the nanoscale level and smaller than the wavelength of the evanescent wave [77]. Compared to SPR, LSPR is more localized and has better spatial sensitivity within the nanometer level [78,79]. In 2014, Sanders et al. designed a LSPR-coupled fiber-optic nanoprobe modified by a mouse anti-human prostate specific antigen (PSA) monoclonal antibody for free PSA detection [80]. Lepinay et al. present a tilted fiber Bragg grating coated with gold nanocages or gold nanospheres, decreasing the minimum detected target concentrations from 90 nM to 11 pM and 8 pM, respectively [81]. Although these metallic nanostructures offer the unique effects of LSPR with strong electromagnetic field confinement, it is still very challenging to precisely control the nanostructures. To overcome this problem, Urrutia et al. proposed a novel facile method to deposit gold nanoparticles to a tapered fiber with a LoD of 271 pM in 2016. They used the LBL-ESA method consisting of polycation (poly[allylamine hydrochloride]; PAH) and negatively charged SiO2 nanoparticles, which endows the sensing region with high porosity, resulting in increased sensitivity [63]. However, the traditional (3-aminopropyl)trimethoxysilane

(APTMS) method and the LBL-ESA method led to a high fraction of AuNP aggregates and uneven distribution. In 2018, Lu et al. demonstrated a new method relying on a poly(styrene-b-4-vinylpyridine) (PS-b-P4VP) block copolymer brush layer to immobilize AuNPs on the fiber [82], as shown in Figure 5a. The presence of the hydrophobic PS blocks seemed to prevent the aggregation of AuNPs. As shown in Figure 5b–e, in comparison with the other two, the PS-b-P4VP templating method drastically reduced the aggregation as well as increased the surface coverage of the AuNPs. The even distribution, orientation, and the high coverage of AuNPs can increase the sensitivity of both the resonance shift and intensity change. In 2019, King et al. took active control of a nanoscale metal by utilizing focused ion beam milling to pattern nanostructures from the deposited metallic thin film [83]. The scanning electron microscope (SEM) image and schematic view are shown in Figure 5f. This process allows the nano-scale control of the dimensions of the metal structures, and they measured PSA to 0.1 pg/mL.

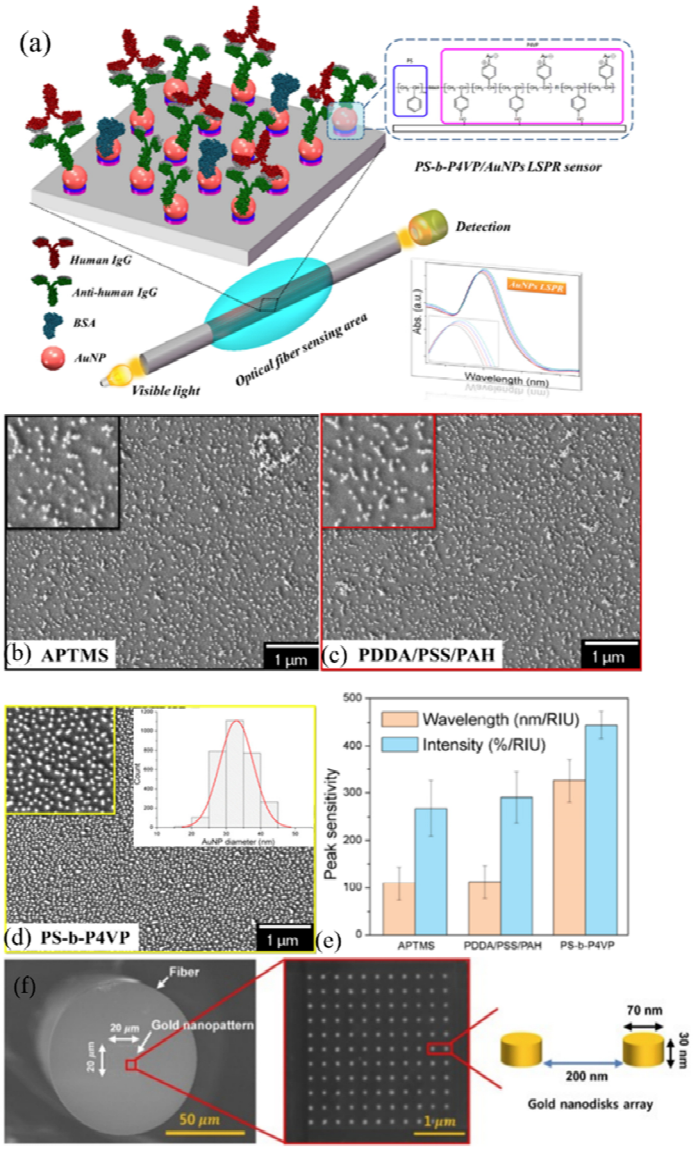

Figure 5. (**a**) Schematic diagram of the PS-b-P4VP-modified LSPR sensor. SEM images of AuNPs templated by (**b**) APTMS, (**c**) LBL-ESA, and (**d**) a PS-b-P4VP brush layer. The diameter of AuNPs is normally distributed. (**e**) RI sensitivities of wavelength and intensity for the three deposition methods. (**f**) SEM image of the Au nanodisk array structure fabricated by the focused ion beam technique and its schematic view. Reprinted with permission from [82,83].

Recently, a novel type of SPR effect, long-range surface plasmonic resonance (LRSPR), has attracted increasing attention due to its narrow half-maximum and high figure of merit (FOM; the ratio between the sensitivity and the half-maximum) [84]. LRSPR is characterized by a dielectric buffer layer between the fiber and the metal thin film. As compared with conventional SPR, LRSPR has longer propagation and deeper penetration [85]. In 2021, Cheng et al. modified a side polished fiber with Au nanoshells, detecting HIgG with a LoD of 0.2 μg/mL [86]. In the same year, Jing et al. demonstrated a LRSPR biosensor modified with a double-antibody sandwich immunoassay for HIgG detection with a LoD of 0.11 μg/mL [87].

LMR Sensors

LMR is explained as a coupling between dielectric waveguide modes and a lossy mode of the coated thin film that occurs when not only the real part of thin-film permittivity must be positive and higher than the imaginary part but also the permittivity of the dielectric needs to be higher than the thin film [88,89]. Typical materials include metal oxides [90], polymer coatings [91], and metal oxides/polymer combined coatings [92]. Indium tin oxide (ITO), ZnO, and SnO2 are all commonly used metal oxides. Among them, ITO, which is a hybrid material, has attracted much attention due to not only having the highest sensitivity but also the fact that SPR and LMR can both exist in ITO [93,94]. It can generate SPR at long wavelengths and LMR at short wavelengths. The polymer coatings, such as PAH/poly-acrylic acid (PAA) or PAH/poly(styrene sulfonate) (PSS), are usually obtained through the LBL-ESA technique, which offers a homogeneous surface coverage for the binding of proteins.

The development of LMR-based optical biosensors is still in the preliminary stage [95]. Currently, compared to SPR biosensors, there are not many studies about biosensors based on LMR. The schematic diagrams of LMR sensor structures are shown in Figure 4f–i. The first time that LMR was utilized to study a protein reaction was when Socorro et al. designed a reflective cladding removed multimode optical fiber coated by a PAH/PSS thin film based on the LBL-ESA technique for IgG detection in 2012 [96]. They achieved visualizing wavelength displacements of 10 nm for a 50 μg/mL concentration. Then, in 2014, they achieved a tapered SMF also modified by the LBL-ESA technique for anti-gliadin antibody (AGA) detection with a LoD of 5 μg/mL [97]. The reduction in the LMR spectral width is an important element, since a broad resonance leads to a higher LoD. In this study, they proved that a narrower and higher attenuation LMR spectrum was obtained by the tapered MMF structure. However, they still only monitored the protein reaction at a fixed concentration. In 2016, Zubiate et al. proposed a fast and reusable D-shaped optical fiber biosensor modified by a hybrid layer of ITO/PAH/PSS and C-reactive protein (CRP)-specific aptamer for CRP detection with a low LoD of 0.0625 mg/L and a fast response time of 61 s [26]. In 2018, Chiavaioli et al. showed a novel poly(methylmethacrylate) polymer (Eudragit L100) and SnO2-coated D-shaped SMF for IgG/anti-IgG assay with a femtomolar LoD of 0.15 ng/L (1fM) in serum [23]. The Eudragit L100 not only provided the necessary carboxylic functional groups (-COOH) on the SnO2 thin-film surface for antibody immobilization but also was regenerated multiple times by injecting sodium dodecyl sulfate. A more simple MCM fiber biosensor modified with the same coatings was presented by Vicente et al. in the next year [98], but they only attained a LoD of 0.6 mg/L for goat anti-mouse IgG detection.

Although the LMR phenomenon has only been applied in optical fiber biosensors for 10 years, compared to the decades of development of SPR sensors, LMR-based fiber sensors show broad prospects in many fields. Many different structures have been proposed, including unclad MMF, tapered SMF, D-shaped fiber, and hetero-core fiber. Based on the novel sensing principle, an ultrahigh sensitivity down to fM level for IgG detection had been achieved. However, LMR sensing techniques still need to be improved in terms of detection costs, practicability, robustness, etc. In view of the continuous sensitivity improvement during recent years, LMR-based biosensors are ideal candidate platforms

for future optical fiber sensors. Some important EMR-based fiber biosensors for protein dection are summerized in Table 2.

Table 2. EMR-based fiber biosensors for protein detection.

Fiber Sensor Configuration	Detection Target	Functionalization Method	Sensitivity	Limit of Detection	Ref
D-shaped plastic optical fiber (POF)	S-RBD	Au film/streptavidin coating + antibody	-	37 nM	[64]
Unclad PCS fiber	HIgG	ELP Au film/PDA/antibody	0.41 nm/(μg/mL)	~2 μg/mL	[27]
TFBG	HIgG	Au film/GO/SPA + antibody	0.096 dB/(μg/mL)	0.5 μg/mL	[33]
Unclad fiber	BSA	Ag film/multi-walled carbon nanotube + MIP	0.862 nm/(ng/L)	0.386 ng/L	[36]
Unclad PCS fiber	HIgG	Ag film/GO + antibody	0.4985 nm/(μg/mL)	0.04 μg/mL	[74]
Tapered fiber	SV	AuNPs/PAH/SiO_2 + biotin	-	271 PM	[63]
PCS fiber	HIgG	PS-b-P4VP block copolymer /AuNPs + antibody	0.036 nm/(ng/cm^2)	1.2 nM	[82]
MMF	PSA	FIB milled nanopatterned AuNPs + antibody	-	0.1 pg/mL	[83]
D-shaped fiber	HIgG	PDA/Au-nanoshells + antibody	1.84 nm/(μg/mL)	0.20 μg/mL	[86]
Reflective unclad MMF	IgG	PAH/PSS + antibody	-	~50 μg/mL	[96]
Tapered SMF	AGA	PAH/PSS + antigen	-	~5 μg/mL	[97]
D-shaped SMF	CRP	ITO/PAH/PSS + antibody	-	0.0625 mg/L	[26]
D-shaped SMF	IgG	Eudragit L100/SnO_2 + antibody	-	0.15 ng/L	[23]
MCM fiber structure	Goat anti-mouse IgG	Eudragit L100/SnO_2 + antigen	-	0.6 mg/L	[98]

2.2.2. Interferometric Sensors

There are many kinds of interferometric optical fiber sensors used for protein biosensing, mainly including the Mach–Zehnder interferometer (MZI), Michelson interferometer (MI), Fabry–Perot interferometer (FPI), Sagnac interferometer (SI), and optical microfiber coupler (OMC).

MZI-Based Fiber Biosensors

MZI is the most studied optical fiber configuration. The transmission spectrum of MZI is based on the phase difference between two light beams. Thus, the intensity of the transmitted light of the MZI can be expressed as:

$$I = I_1 + I_2 + 2\sqrt{I_1 I_2}cos\Delta\varphi \quad (2)$$

$$\Delta\varphi = \frac{2\pi}{\lambda}\left(n_{eff,1}L_1 - n_{eff,2}L_2\right) \quad (3)$$

where I_1 and I_2 are the intensities of the two interfering light beams, λ is the wavelength of the injected light, $n_{eff,1}$ and L_1 are the effective RI and propagation length of light beam 1, $n_{eff,2}$ and L_2 are the refractive index and propagation length of light beam 2, and $\Delta\varphi$ is their phase difference. The m-order interference intensity minima, $\lambda_{min,m}$, occurs when:

$$\lambda_{min,m} = \frac{2\left(n_{eff,1}L_1 - n_{eff,2}L_2\right)}{2m+1} \quad (4)$$

where m is an integer.

In biosensors, the biomedical reactions will change the effective refractive indices of the two lights discrepantly. By monitoring the wavelength shifts of the dips in the spectra, the concentration of the analyte can be detected. The typical fiber MZI sensor is shown in Figure 6a–g. Generally, there are three methods to generate the phase difference, including different light paths, intermodal dispersion, and birefringence. Different light paths can result from core-offset fibers [99,100], microstructured optical fibers [101,102], S-tapered fibers [103], and hetero-core fibers [21]. In 2018, Yang et al. used a twin-core hollow optical fiber to fabricate an optofluidic biosensor [104]. Figure 7a,b shows the

schematic diagrams of the biosensor structure. Tapered fiber structures are widely used for causing modal dispersion. The mode interference in MFs is mainly between the HE11 and HE12 modes [7,105–107]. In addition to microfibers, Ravikumar et al. presented an interferometric biosensor based on a chitosan (CS)–nickel (Ni) film-coated no-core fiber (NCF) spliced between two single-mode fibers (SMFs) for hexa-histidine-tagged microcin (His-MccS) detection [108]. The higher order modes are excited by the fundamental mode of the injected light within the NCF region, and the interference occurs between these modes [109]. The birefringence method is based on the interferometer between p- and s-polarization light. Currently, only Huong et al. studied the birefringence interferometer biosensor for protein detection based on the SPR technique [110]. MZI-based optical fiber sensors have a series of advantages, such as high sensitivity, good stability, and real-time measurement in vitro. However, MZI is a transmission type interferometer, thus it is difficult to achieve plug-in measurements, which limits the application of these sensors to in vivo measurements [111].

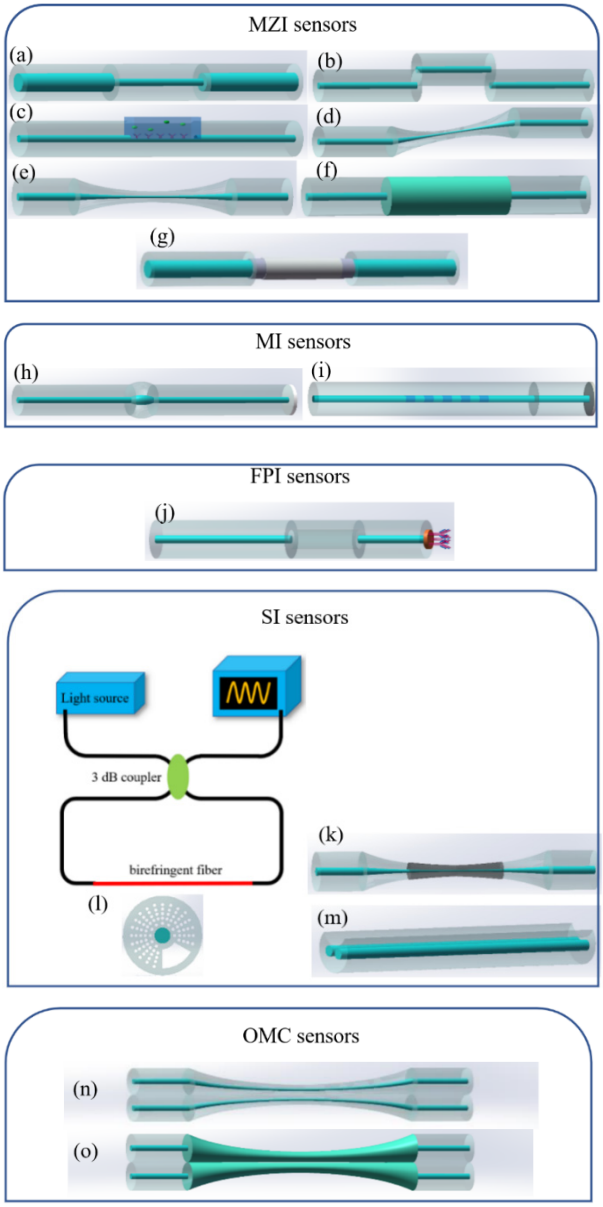

Figure 6. The schematic diagrams of (**a**–**g**) the MZI sensors, (**h**,**i**) MI sensors, (**j**) FPI sensors, (**k**–**m**) SI sensors, and (**n**,**o**) OMC sensors.

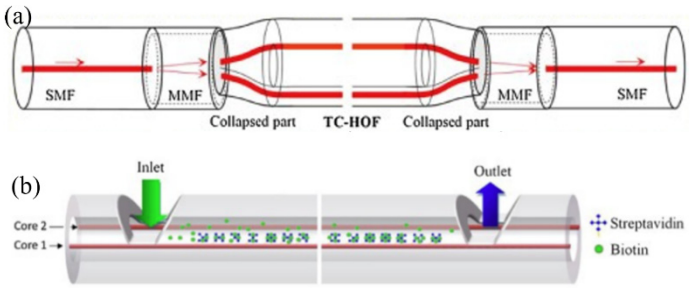

Figure 7. Schematic diagrams of the (**a**) structure and (**b**) microfluidic path of twin-core hollow optical fiber. Reprinted with permission from [104].

MI-Based Fiber Biosensors

The typical structures of fiber MI sensors are shown in Figure 7h,i. In contrast to fiber MZI sensors, interference occurs between reflected light beams instead of transmitted light beams. The light injected into the fiber input port is divided into two beams in the coupler, reflected at the reflective end face of the fiber after transmission, and finally recoupled from the original path back to the input port for output. The phase difference of the reflected light of the MI can be expressed as:

$$\Delta\varphi = \frac{2\pi}{\lambda}\left(n_{eff,1} \cdot 2L - n_{eff,2} \cdot 2L\right) \quad (5)$$

where L is the propagation length of both light beam 1 and light beam 2. To date, there are three coupling methods used for protein biosensing, including employing long-period grating [112], waist-enlarged fusion taper [113], and dual-core fiber [114]. Usually, the sensing region is located at the fiber surface, and the bio-reaction will change the effective RI of the cladding mode. In 2018, Wysokiński et al. demonstrated a dual-core all-fiber (DCF) configuration for protein antigen detection, achieving a peak shift of 0.6 nm [114]. Figure 8b is the SEM image of DCF; since the cores are closer to each other, the sensor exhibits good resistance to temperature and stain changes. Most importantly, as shown in Figure 8a, the sensing region is located at the probe tip, which contributes to the sensing in vivo without tissue dissection. In brief, the size of the reflective fiber MI sensors is further decreased compared to fiber MZI sensors, which provides great convenience for practical application.

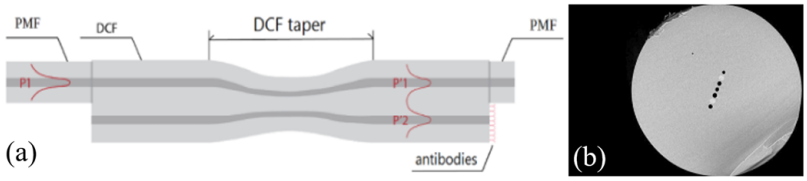

Figure 8. (**a**) Schematic diagram of tapered DCF structure and (**b**) SEM image of DCF. Reprinted with permission from [114].

FPI-Based Fiber Biosensors

Fiber FPI sensors, which are also a refractive structure, are based on the theory of parallel plate multi-beam interference [115,116]. The injected light reflected by multiple reflection interfaces results in multiple light beams, and interference occurs due to the phase difference between these light beams. Compared to two reflection interfaces, FPI with three or more reflection interfaces possesses more than two cavities, resulting in better accuracy [117]. The typical structure of a FPI protein biosensor is shown in Figure 6i.

According to the interference intensity equation of reflective light beams in the case of a single cavity, the interference spectrum in the case of two cavities can be expressed as:

$$\begin{aligned} I = [I_1 + I_2 + 2\sqrt{I_1 I_2}\cos\left(\tfrac{4\pi nL}{\lambda}\right)] \\ + \left[I_1 + I_s + 2\sqrt{I_1 I_s}\cos\left(\tfrac{4\pi nL + 4\pi n_s L_s}{\lambda}\right)\right] \\ + \left[I_2 + I_s + 2\sqrt{I_2 I_s}\cos\left(\tfrac{4\pi n_s L_s}{\lambda}\right)\right] \end{aligned} \quad (6)$$

where I_1, I_2, and I_s are the reflective intensities correspond to the three reflections in sequence; n and L are the effective index and length of the first cavity, respectively; n_s and L_s are the effective index and length of the sensing cavity, respectively; and λ is the free-space wavelength. The Fabry–Perot 1 (FP1) cavity is a special air cavity, such as hollow core fiber (HCF) [117,118] or hollow-core photonic crystal fiber (HCPCF) [119], with a fixed length. The Fabry–Perot 2 (FP2) cavity is the sensing cavity that usually immobilizes the biomolecule receptors on the end face of the FP2 cavity. When the protein ligands bind to the receptors, the combined protein can be regarded as forming a thin protein film resulting in extending the thickness of L_s and modulating the effective RI n_s. However, Xie et al. proposed a novel fiber FPI biosensor structure of two separate cavities [120]. Each FP cavity was splicing a C-shaped fiber between two SMFs, and the results showed minimal cross-talk between them. Individual interferences corresponding to each FPI cavity can be separated utilizing fast Fourier transform. In this case, if a cavity is utilized as a negative control, false positive measurements will be greatly reduced. In general, in comparison to MZI and MI, FPI is extraordinarily sensitive because of multiple reflections in interference. Meanwhile, it gets rid of the limitation of the coupler section, which might lead to complex processing operations and data analysis. In addition, a broader bandwidth light allows using shorter cavities, which make it more suitable for sensing in vivo.

SI-Based Fiber Biosensors

In contrast, due to the fragile fiber structure and the large size of the system [121,122], SI is relatively less studied in biological sensing. The injected light from a broadband source is split into clockwise and counter-clockwise light beams by a three dB coupler as it enters the loop. After light passes through the polarization controller, the x or y polarization of counter-propagating beams are transformed into the opposite. A net phase difference is accumulated as the two polarized lights propagate through the length of the birefringent fiber, resulting in interference given by the recombination at the coupler [122]. The transmission ratio of optical intensity injected into the SI can be expressed as:

$$T = \frac{1 - \cos\varphi}{2} \quad (7)$$

$$\varphi = \frac{2\pi B(\lambda, n) L_b}{\lambda} \quad (8)$$

where $B(\lambda, n)$ is the birefringence of the birefringent fiber, and L_b is the length of the birefringent fiber. The structures of SI protein biosensors are shown in Figure 6k–m. In biosensors, the birefringent fiber is usually an ultra-thin tapered fiber. The smaller size of the microfiber corresponds to higher birefringence, leading to the higher sensitivity of the SI sensor. Wang et al. presented a cascaded SI biosensor based on the Vernier effect for BSA detection with a sensitivity of 9.097 nm/(mg/mL) [123] in 2018. Nonetheless, Zhang et al. designed and fabricated a side-channel photonic crystal fiber and detected the human cardiac troponin T (cTnT) in in-line optofluidic configurations [22]. Li et al. utilized exposed core microstructure optical fiber (ECF) as a birefringent fiber, achieving streptavidin recognition [124]. The schematic diagram of the system is shown in Figure 9a. Figure 9b shows a cross-sectional image of the ECF, whose suspended core is exposed to the surrounding medium, forming an optofluidic channel. In sum, the fragile problem and

large ring structure increase the application difficulty of fiber SI sensors; however, it still has the potential to achieve real-time measurement in vitro for its ultra-high sensitivity.

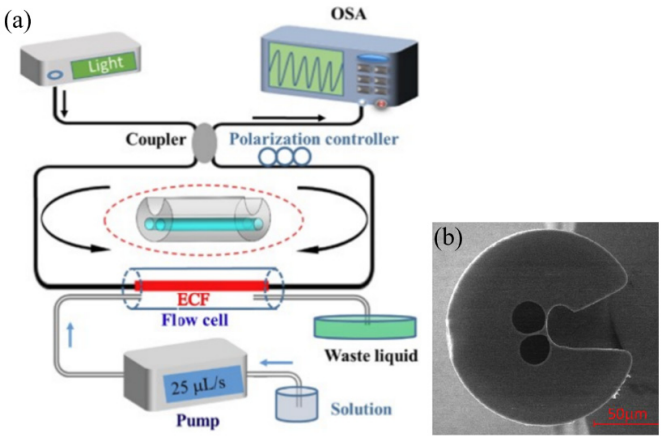

Figure 9. (**a**) The schematic diagram of an ECF-based SI biosensor system, and the (**b**) SEM image of ECF. Reprinted with permission from [124].

OMC-Based Fiber Biosensors

The structures of coupler-based optical fiber biosensors are typically the OMC, as shown in Figure 6n–o, which are fabricated by tapering and fusing two physically contacted fibers together at the same time. The fused fibers include SMFs and hetero-core structure fibers.

In the case of SMFs, according to the supermode theory [125], the two microfibers are regarded as a new waveguide. When the polarized light with power, P_1, is injected into port 1, both the odd and even supermodes are simultaneously excited and couple with each other. The output power in port 3 and port 4 can be expressed as:

$$P_3 = P_1 \cos^2\left[\frac{\pi L\left(n_{eff,even} - n_{eff,odd}\right)}{\lambda}\right] \tag{9}$$

$$P_4 = P_1 \sin^2\left[\frac{\pi L\left(n_{eff,even} - n_{eff,odd}\right)}{\lambda}\right] \tag{10}$$

where L is the coupling length, λ is the wavelength of the transmitted light, and $n_{eff,even}$ and $n_{eff,odd}$ are the effective RI of the even supermode and odd supermode, respectively. When the biological reaction happens in the coupling region, the coupling process is influenced due to the variation in RI and thinness. In the early years, biosensors based on OMC structure were used for SV [126] and anti-fibrinogen [127] detection. In 2018, Zhou et al. adjusted the working point around the dispersion turning point by carefully designing the dimension of OMC, achieving the detection of cardiac troponin I (cTnI) with a LoD of 2 fg/mL [128]. In the same year, Li et al. demonstrated a fiber-optic modal interferometer with birefringence-induced Vernier effect based on OMC [129]. As shown in Figure 10, the dips with the Vernier effect exhibit a much stronger redshift with the same surrounding RI increment, which demonstrates the great contribution of the Vernier effect for sensitivity enhancement.

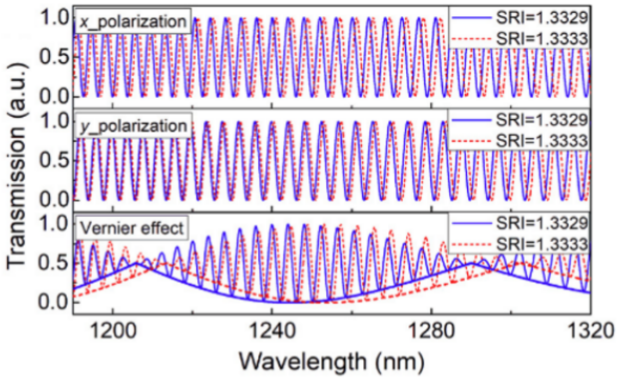

Figure 10. The wavelength shifts comparison of x-polarization, y-polarization, and with the Vernier effect. Reprinted with permission from [129].

In 2020, Chen et al. employed single-mode–no-core–single-mode (SNS) fiber instead of SMF to fabricate the OMC [130]. When the light is transmitted from input SMF to tapered NCF, multiple modes are excited and coupled to the other NCF. The tapered SNS fiber coupler possesses better stability without sacrificing sensitivity since the tapered coupler structure is composed of two fibers. They successfully detected inactivated *Staphylococcus aureus* with a LoD of 3.1 CFU/mL.

Phase-modulation-based biosensors are diverse, with good stability and high sensitivity. With the introduction and application of the Vernier effect, the sensitivity of biosensors has been further improved. Relying on signal processing technology, the sensors based on the Vernier effect in a single interferometer became possible [131]. This will greatly reduce the complexity of the sensor system and provide tremendous potential for protein biosensing applications. Some important interferometer-based fiber biosensors for protein dection are summerized in Table 3.

Table 3. Interferometer-based fiber biosensors for protein detection.

Interferometric Type	Fiber Sensor Configuration	Detection Target	Functionalization Method	Sensitivity	Limit of Detection	Ref
MZI	SMF-thin core SMF-SMF	SV	PDDA/PSS + biotin	-	0.02 nM	[21]
	Core offset SMF	HIgG	SPA + antibody	-	47 ng/mL	[99]
	S-tapered SMF	HIgG	PDA/SPA + antibody	-	28 ng/mL	[103]
	Microcavity	BSA	None	−38.9 nm/(mg/mL)	0.257 µg/mL	[101]
	Twin-core hollow optical fiber	biotin	SV	16.9 nm/(mg/mL)	~10 µg/mL	[104]
	SMF	CRP	PDA + MIP	0.881 nm/(lg ng/mL)	5.813×10^{-10} ng/mL	[107]
	SMF-NCF-SMF	His-MccS	CS-Ni film	0.0308 nm/(ng/ml)	0.8368 ng/ml	[108]
MI	Unclad MMF	CRP	TiO_2/Ag/Al + antibody	-	10 ng/mL	[110]
	waist-enlarged fusion taper	Anti-IgG	CS/PSS + antigen	5.91 nm/(ng/mm^2)	4.941 nM	[113]
	Tapered dual-core all-fiber	Rabbit IgG	Antibody	-	~4 µg/mL	[114]
FPI	SMF + HCF	IgG	CS/polystyrene sulfonate membrane + antibody	0.033 µm/(pg/mm^2)	0.005 nM	[118]
	SMF+HCPCF+SMF	Rabbit IgG	Antibody	-	~0.1 µg/mL	[119]
	Two cascaded C-shaped fibers	SV	PAH/PSS + biotin	-	61 µg/mL	[120]
SI	MF	BSA	GO	9.097 nm/(mg/mL)	-	[123]
	Photonic crystal fiber	cTnT	Antibody	-	1 ng/mL	[22]
	Exposed core fiber	SV	PAS/PSS + biotin	-	~0.2 mg/mL	[124]
OMC	Coupled SMF	Anti-fibrinogen	Antigen	-	~25 µg/mL	[127]
	Coupled SMF	cTnI	PDDA/PAA + antibody	-	2 fg/mL	[128]
	Coupled SMF	cTnT	PAA + antibody	-	1 ng/mL	[129]
	Coupled SNS fiber	*S. aureus*	Pig IgG antibody	-	3.1 CFU/mL	[130]

2.2.3. Fiber Grating Sensors

Fiber gratings are periodic modulations of the RI of the fiber core in the longitudinal direction, forming an optical filter [132], and the most widely used method for fabricating fiber gratings is the phase mask technique [133]. According to the period of the modulation

period, fiber gratings can be divided into fiber Bragg gratings (FBGs) and long period gratings (LPGs).

FBG-Based Fiber Biosensors

The schematic diagram of FBGs is shown in Figure 11a. The modulation period of the FBGs is on the order of hundreds of nm. At the FBGs, a narrow spectral band is reflected, and the remaining light is transmitted. The wavelength of the reflected light, which is called the Bragg resonance wavelength (λ_B), is defined by the Bragg phase matching condition [134]:

$$\lambda_B = 2n_{eff}\Lambda \tag{11}$$

where n_{eff} and Λ are the effective RI and the grating period, respectively. The interaction between the surrounding analyte and functionalized FBG surface can lead to the change of the RI, thus resulting in the effective RI change of the fiber mode. Then, the target analyte can be detected by monitoring the wavelength shift of the Bragg resonance wavelength. FBG itself is not suitable for RI sensing. In biosensing for protein detection, only Srinivasan et al. utilized relatively simple, bare FBG (bFBG) for the detection of *Escherichia coli* bacteria [135]. Most of the studies normally employ modified FBG, such as etched fiber Bragg grating (eFBG) and tilted fiber Bragg grating (TFBG), as shown in Figure 11b,c. The fabrication method of the eFBG is commonly chemical etching with hydrofluoric acid (HF). A section of FBG is immersed in HF to remove its cladding. Several works show that the RI sensitivity of eFBG sensors increases with the increased etching of the cladding layer, which provides the tunability of the sensitivity [136,137]. In 2015, Sridevi et al. designed an eFBG sensor coated with GO for CRP detection with a LoD of 0.01 mg/L [138]. In 2018, Bekmurzayeva et al. presented an eFBG sensor functionalized with aptamer for thrombin detection [139]. In the same year, Schulze et al. fabricated the eFBG for CRP detection via ultrafast-laser-inscription [140]. In comparison with the phase mask technique, it is more flexible in creating different gratings due to the tuneable translation speed during the inscription process [141,142], which is beneficial for customizing the desired biosensor.

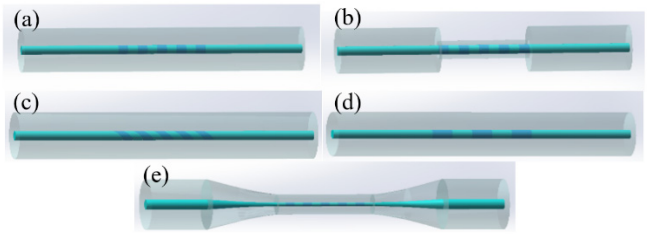

Figure 11. The schematic diagrams of (**a**) FBG, (**b**) etched FBG, (**c**) tilted FBG, (**d**) LPG, and (**e**) tapered fiber grating.

Another variant of FBG is TFBG, whereby a small angle with the optical axis causes the coupling of optical power from the forward-propagating core mode into a multitude of cladding modes [143]. The m-th resonance position $\lambda_{clad,m}$ can be calculated from [144]:

$$\lambda_{clad,m} = \frac{(n_{core,m} + n_{clad,m})\Lambda}{cos\theta} \tag{12}$$

where $n_{core,m}$ and $n_{clad,m}$ are the effective RI of the core and cladding mode, respectively, and Λ and θ are the period and the internal tilt angle of the TFBG, respectively. The resonance transmission spectrum of a TFBG is modified by the surrounding RI. The resonances related to propagation modes with an effective RI lower than the external will not be guided [145]. The first TFBG sensor for protein detection was proposed by Maguis et al. in 2008 [146]. Then, Luo et al. utilized excessively tilted fiber grating (Ex-TFG), whose θ is larger than 70°, modified with SPA for immunoassay analysis in 2016 [13,147]. Recently, Sun et al. achieved a sensitivity and detection range adjustable biosensor by utilizing the

correlation between the cladding resonance peak and the external RI [148]. Moreover, the most widely used TFBG biosensors are combined with SPR [33,149–155] or LSPR [156–158] technology. The Au thin-film and AuNPs greatly enhance the impact of the analyte on the fiber cladding mode via the SPR or LSPR effect. Meanwhile, since the Bragg mode is insensitive to the surrounding medium but sensitive to the temperature, the temperature variation can be self-calibrated [159]. Lao et al. proposed a TBFG biosensor employing a new mechanism comprising hybrid excitation of both long-range and localized SPRs for thrombin detection with a LoD of 1nM [157]. The several cladding resonances generated by SPR in the wavelength range of 1485 nm to 1510 nm are sensitivity to RI and temperature, while the core mode near the wavelength of 1555 nm is not affected by RI but is sensitive to temperature. In conclusion, TFBG and SPR-assisted TFBG sensors are both more sensitive than eFBG sensors. However, eFBG sensors have the advantage of ease of fabrication, sensitivity tunability, and a lack of a need for polarization control. In 2019, Sypabekova et al. detected thrombin by etched TFBG, which shows improved sensitivity and does not require polarization control [160].

Bragg grating written in microfiber (mFBG) is also competitive for its purity of mode-coupling, relatively narrow bandwidth signal, and multiplexing capability [161]. Liu et al. demonstrated a phase-shifted microfiber Bragg grating (PS-mFBG) for cTnI detection [162]. The π-phase-shift in modulation provided a narrow-band notch signal to the reflective spectrum, which greatly improved the resolution of the mFBG. Ran et al. exploited a harmonic mFBG to offset the impact of temperature without an additional sensing element in 2021 [163].

LPG-Based Fiber Biosensors

The LPG is another period-modulated grating structure, wherein the period typically ranges from 100 to 1000 μm [164], and the schematic diagram of LPG is shown in Figure 11d. It couples the light from fundamental core mode to the forward propagating cladding modes. A discrete set of resonant bands appear in the transmission spectrum, and the center wavelengths λ_m of these attenuation bands are given by the phase-matching condition [165]:

$$\lambda_m = (n_{core} - n_{clad,m}) \cdot \Lambda \tag{13}$$

where n_{core} and $n_{clad,m}$ are the effective RI of the core and the m-th cladding mode, respectively, and Λ is the period of the grating. As a result, the mechanism provides the possibility of sensing the surrounding RI caused by the biological recognition events. Since Matthew et al. proposed the first LPG biosensor for HIgG detection in 2000 [166], LPGs based on all kinds of coating materials, such as Eudragit L100 [167], titanium oxide (TiO_x) thin-film [168], poly(methylmethacrylate)-co-methacrylic acid (PMMA-co-MA) [169,170], and GO [171–173], are employed for protein fiber sensing. However, the highest sensitivity range of LPG is close to the RI of fiber cladding (i.e., 1.45 RIU), which is far from the RI range of the aqueous solution (i.e., 1.33 RIU). Diverse methods have been adopted to solve this problem. One of the most popular configurations involves coating high-refractive-index materials on the fiber surface to make the devices work in the mode transition (MT) region. It is proven that the attenuation band moves to a lower RI region as the overlay thickness increases [174]. A fundamental feature of this mechanism is the possibility to tune the attenuation band to about 1.33 RIU by controlling the thin-film thickness. Pilla et al. first utilized atactic polystyrene (PS)-coated LPG for SA detection in 2009 [175]. Subsequently, various materials are used as a high-refractive-index layer in MT-LPG sensors. In 2015, Chiavaioli presented a LPG sensor based on sol-gel-based titania-silica thin-film for anti-IgG detection [176]. In 2018, Esposito et al. tuned the working point through a multilayer system consisting of polycarbonate (PC) film and a much thinner GO layer for biotinylated BSA (bBSA) detection [177]. In particular, as a secondary effect, the resonance depth will be reduced by a few dB during MT, which can affect the visibility of the attenuation bands. To address the above challenge, Esposito et al. demonstrated an unconventional LPG fabricated in a GO-coated double cladding fiber with a W-shaped RI profile in 2021 [178],

whose structure is shown in Figure 12. This device is tested for the real-time label-free detection of CRP in serum with a LoD of 0.15 ng/mL.

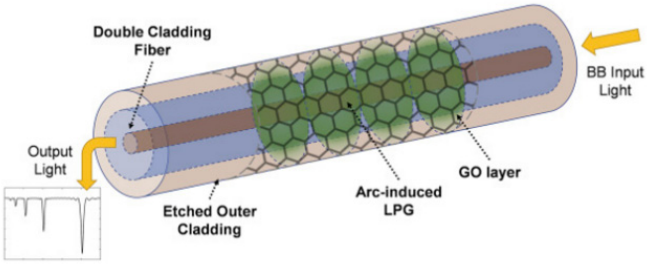

Figure 12. The schematic diagram of a MT-LPG biosensor with W-shaped RI profile. Reprinted with permission from [178].

Despite the outstanding novelty of MT-LPG sensors, the process of the overlay deposition is costly and time-consuming. Another approach, which couples the propagating core mode with a high-order cladding mode near its turn-around point (TAP), was proposed for increasing the sensitivity of LPG [179,180]. The relationship between the grating period and the resonance wavelength can be described by the phase-matching curves. The slope of curves for a higher order mode shows a sign change from positive to negative, and the TAP is defined as the point where the slope of a specific PMC is near to 0. When the working position is near the TAP, there are two resonant bands showing the highest sensitivity with opposite movement direction. The total wavelength shift is the sum of the wavelength shift of the two resonance bands. In this case, only the coating thickness needs to be carefully selected to ensure the best sensitivity. In the past several years, TAP-LPGs have been fabricated by etching [181] or coating with different kinds of materials, such as GO [19] and Eudragit L100 [182]. From 2016 to 2018, Marques et al. studied the TAP-LPG modified with PAH/gold shell-coated silica nanoparticles (SiNPs) using the LBL technique for human immunoglobulin M (HIgM) [44,183]. In 2021, Dey et al. fabricated the Eudragit L100-coated LPG with lowest order cladding mode $LP_{0,2}$ near TAP by reducing the cladding diameter of LPG down to ~20 µm [184]. Piestrzyńska et al. proposed a MT and TAP effect combined LPG sensors by precisely controlling the thickness of the deposited TaO_x with the atomic layer deposition method [185]. The response curves of the dual-peak resonant wavelength shift at different avidin concentrations are shown in Figure 13.

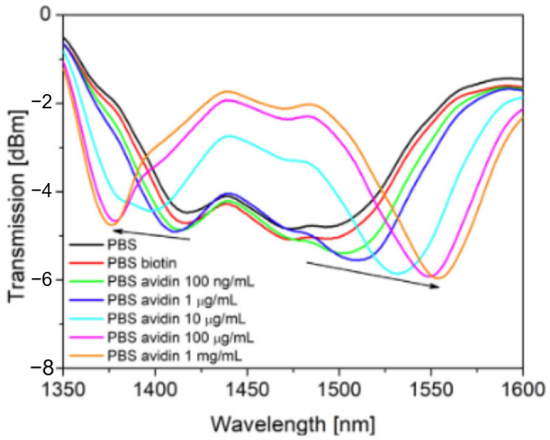

Figure 13. Transmission spectra for TaOx-coated LPG at different avidin concentrations. Reprinted with permission from [185].

In addition to the above methods, in 2021, Lee et al. applied the π-phase-shift technique to LPG, resulting in a splitting of the loss dip at the resonance wavelength [186], and they realized the detection of the SARS-CoV-2 spike protein with a LoD of 100 pg/mL. Zuppolini

et al. reported the reflection-type long period fiber gratings (RT-LPG) for the fast detection of class C β-lactamases expressed by drug-resistant bacteria and also the design and development of an automated system for simultaneous multi-target clinical analyses [170]. In summary, although the sensitivity of LPG sensors is low in an aqueous solution, it can be improved through many methods. Some important grating-based fiber biosensors for protein dection are summerized in Table 4.

Table 4. Fiber grating-based fiber biosensors for protein detection.

Fiber Sensor Configuration	Detection Target	Functionalization Method	Sensitivity	Limit of Detection	Ref
eFBG	CRP	GO + antibody	-	0.01 mg/mL	[138]
eFBG	Thrombin	Aptamer	-	10 nM	[139]
eFBG	CRP	Aptamer	-	0.82 pg/L	[140]
Ex-TFG	NT-proBNP	SPA + antibody	45.967 pm/(ng/mL)	0.5 ng/mL	[13]
TFBG	HIgG	Au film/GO/SPA + antibody	0.096 dB/(μg/mL)	0.5 μg/mL	[33]
TFBG	Thrombin	AuNPs + aptamer	-	1 nM	[157]
etched TFBG	Thrombin	Aptamer	3.3 pm/nM	0.075 nM	[160]
PS-mFBG	cTnI	Polyelectrolyte + antibody	-	0.03 ng/mL	[162]
harmonic mFBG	cTnI	Antibody	-	13.5 ng/mL	[163]
LPG	Anti-IgG	Eudragit L100 + antigen	-	500 ng/mL	[167]
U-bent LPG	HIgG	GO + antibody	-	23 ng/mL	[172]
Micro-tapered LPG	Hemoglobin	GO + antibody	0.73 nm/(mg/mL)	0.02 mg/mL	[173]
MT-LPG	bBSA	PC/GO + SV	-	0.2 aM	[177]
Double cladding MT- LPG	CRP	GO + antibody	−19.22 nm/(μg/mL)	0.15 ng/mL	[178]
TAP-LPG	Anti-IgG	GO + antigen	-	7 ng/mL	[19]
TAP-LPG	HIgM	PAH/gold coated SiNPs + antibody	11 nm/(ng/mm^2)	15 pg/ mm^2	[183]
Etch TAP-LPG	Anti-IgG	Eudragit L100 + antigen	-	0.16 ng/ml	[184]
MT and TAP LPG	avidin	TaO_x + biotin	10.21 nm/log(ng/ml)	-	[185]
PS-LPG	SARS-CoV-2 spike protein	antibody	-	100 pg/mL	[186]

NT-proBNP: N-terminal pro-B-type natriuretic peptide.

2.3. Scattering-Based Fiber Biosensors

Optical scattering describes a physical process wherein light is forced to deviate from a straight trajectory by non-uniformities in the medium through which it passes. According to whether the frequency of the scattered light changes, the scattering can be divided into elastic and inelastic scattering. In optical fiber-based protein sensors, the widely used scattering mechanisms include surface-enhanced Raman scattering (SERS) and Rayleigh backscattering.

Raman scattering is one of the elastic scatterings, and SERS is a surface-sensitivity technique that enhances the intensity of the Raman spectra of molecules adsorbed on rough metal surfaces or nanoparticles, especially made of gold or silver [187–190]. In particular, Pisco et al. showed self-assembled periodic patterns on the optical fiber tip by microsphere arrays in 2015 [191], and their group achieved tailoring lab-on-fiber SERS optrodes towards biological targets of different sizes recently [192]. In 2020, Kim et al. presented fiber-optic SERS probes fabricated using two-photon polymerization for the rapid detection of bacteria [193]. Due to the advantage of flexibility, optical fibers can be used as SERS probes, which provide the potential ability to detect target analytes in vivo, whereas conventional optical fibers lack the sensitivity needed for biosensing. To address this problem, a hollow-core photonic crystal fiber (HCPCF) is normally used for SERS probes because of its ability to incorporate liquid analytes and metal nanoparticles into the holes [194–196]. In 2007, Zhang et al. first reported on a modified HCPCF that allows for the filling of only the core with molecules in solution with silver nanoparticles for human insulin detection [197]. A similar HCPCF-based SERS sensing platform was further studied by Dinish et al. for the detection of epidermal growth factor receptors (EGFRs) in low sample volume in 2012 [198]. After two years, they achieved the simultaneous detection of hepatocellular carcinoma (HCC) biomarkers AFP and alpha-1-antitrypsin (A1AT) secreted in the supernatant from the Hep3b cancer cell line [199]. In 2019, in order to introduce the optofluid into HCPCF,

Hunter et al. showed an optofluidic label-free SERS platform for rapid bacteria detection in serum [200]. On the other hand, HCPCF is susceptible to a transmission window shift when the air holes are filled with liquid [201]. Yang et al. designed a tip-coated multimode fiber sensor with cetyltrimethylammonium bromide (CTAB)-capped silver nanoparticle (SNPs) coated on the fiber tip for protein detection with a LoD of 0.2 μg/mL [202]. In 2018, Danny et al. functionalized a U-bent plastic optical fiber probe with Raman-active AuNP labels, realizing HIgG detection with a LoD of 0.6 μM [203].

Rayleigh backscattering belongs to elastic scattering. Even in the absence of a reflective element, such as FBG, Rayleigh backscattering will still exist and be detected by optical backscatter reflectometry [204]. Sypabekova et al. investigated an etched MgO-based nanoparticle-doped fiber functionalized by ssDNA aptamer for thrombin detection in 2020 [205]. The schematic diagram is shown in Figure 14a. The MgO-based nanoparticle-doped fiber has a good 'gain' for Rayleigh backscattering, which is made by chemical vapor deposition, wherein the fabrication is cost effective and simplified [206]. When the fiber is etched, Rayleigh scattering is further increased due to more available nanoparticles to cause the scattering. Figure 14b shows a comparison of scattered power before and after etching. Based on this biosensing platform, they detected the thrombin molecule concentrations ranging from 0.625 μg/mL to 20 μg/mL. In 2021, Ayupova et al. developed an optical fiber ball resonator sensor based on Rayleigh backscattering for thrombin detection [207]. Since the RI of the ball resonator is generally higher than the surrounding RI, the light is continuously reflected inside the resonator by total internal reflection and hardly leaves the sphere. The interaction between the light and the analyte is dramatically enhanced by the multiple reflections [208]. The signal from the ball resonator was detected with an optical backscatter reflectometer, which showed a LoD of 1.56 pM.

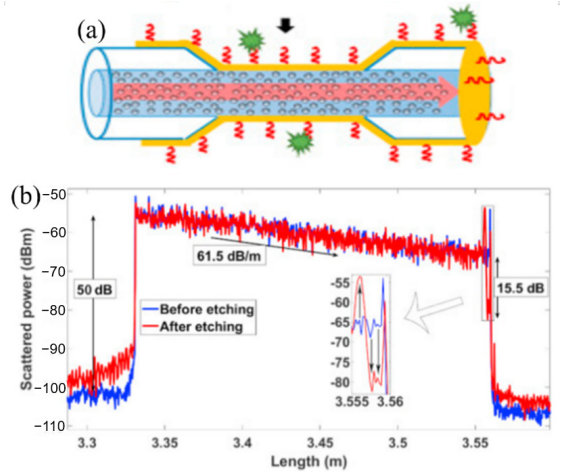

Figure 14. (**a**) The schematic diagram of an etched MgO-based nanoparticle-doped fiber sensor coated by Au film. (**b**) The typical scattering traces with backscattered power before etching and after etching. Reprinted with permission from [205].

Scattering-based optical fiber biosensors have great potential in clinical diagnosis. The performance of these biosensors largely depends on the area of light–analyte interactions, the combined effects of transmission losses, and the scattered signal collection efficiency.

2.4. Fluorescence-Based Fiber Biosensors

Fluorescence is the emission of light by a substance that has absorbed light or other electromagnetic radiation. Some molecules are capable of being excited, via the absorption of light energy, to a higher energy state, also called an excited state, which cannot be sustained for long. It will transition to a lower-energy state, resulting in the emission of light energy. In optical fiber-based bioassay, proteins themselves usually do not generate fluorescent signals and need to be labelled with fluorescent tags, which will be excited by the evanescent wave of the optical

fiber and emit light signals with specific wavelengths [209,210]. The intensity of the emitted light I_f is directly related to the concentration of the fluorescent tags and can be given by [211]:

$$I_f = \mathrm{K}\Phi_f I_0 \alpha bc \tag{14}$$

where K is a constant related to the efficiency between the collection instrument and the emitted light, Φ_f is the fluorescence quantum yield, I_0 is the intensity of the injected light, and αbc are the parameters involved in the Lambert–Beer molecular absorption law. Different from label-free detection, fluorescent label detection adopts the sandwich assay as shown in Figure 15a. 'Capture' antibodies (or first antibodies) were immobilized on the surface of the fiber surface, and fluorescent tags labelled 'detection' antibodies (or secondary antibodies) were added to the bulk solution. When the target antigen is added into the solution, a 'molecular sandwich' is formed on the fiber surface. Then, the fluorescent tags attached to the 'detection' antibodies will be excited by the evanescent wave and produce characteristic fluorescence. It can be seen that one of the keys for a fluorescence sensor is to obtain a good performance of the evanescent field.

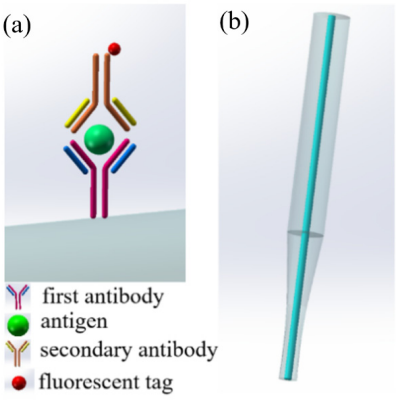

Figure 15. (**a**) The schematic diagram of fluorescent label detection and (**b**) a tapered fiber probe.

The typical structure of the fluorescent sensors is a tapered fiber probe as shown in Figure 15b. The tapered fiber probe is usually gained by immersing a silica fiber with the outer protective sheath removed to an HF solution. The tapered structure shows the increased depth and magnitude of the evanescent field [50,212]. Preejith et al. studied a tapered fluorescent optical fiber for measuring total serum protein in 2006 [213]. The proteins were labelled by NanoOrange, a merocyanine dye reagent, which becomes strongly fluorescent at about 610 nm when excited at about 470–490 nm. In 2009, Kapoor et al. achieved the specific detection of the interleukin-6 (IL-6) protein with a 'sandwich' structure [214]. They used the least square fitting method to subtract the background spectral profile from the total fluorescence signal profile. Therefore, they did not need to treat the probe surface with blocking buffer. In this new strategy, they successfully detected IL-6 protein, down to 5 pM (0.12 ng/mL).

Researchers have also explored other structures to improve the performance of evanescent waves. Padmanabhan et al. utilized a HCPCF structure for estrogen receptor detection [215]. Hsieh et al. amplified the fluorescent signal intensity by a Fabry–Perot resonator structure [216]. Chang et al. proposed a novel optical fiber biosensor based on a localized surface plasmon coupled fluorescence system. They combined the 'detection' antibodies with AuNPs. When the localized surface plasmons are excited by an evanescent wave, a significantly enhanced localized electromagnetic field exists near the AuNPs' surface, resulting in the fluorescent tags being excited by the enhanced localized field of surface plasmons. Based on the sensor, they detected mouse IgG, alpha-fetoprotein (APF), and SARS-CoV-2 N-protein in human serum [25,217,218]. In 2017, Liu et al. directly modified AuNPs on the fiber surface, successfully detecting IL-6 with a LoD of 1 pg/mL [219]. Later, they reduced the LoD down to 0.1 pg/mL with the help of biotin–streptavidin coupling [220]. The biosensor exhibits good spatial resolution of 200 μm. As shown in Figure 16, when

different concentrations of IL-6 were dropped on two locations of the fiber, different intensities of fluorescence can be observed, which indicated that the fiber could discriminate between different concentrations at different locations. In 2016, Chang et al. demonstrated a liposome-based total internal reflection fluorescence fiber-optic biosensor [221]. Liposomes act as signal amplifiers. Each liposome contained more than 1×10^5 molecules of fluorescent tags, which significantly enhanced the intensity of the emitted fluorescence signal. Their system realized 0.2 pg/mL of IgG detection.

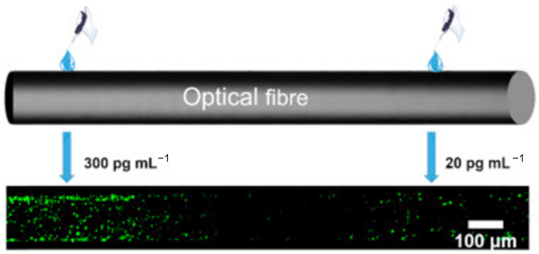

Figure 16. Localized determination of IL-6 by dropping two different concentrations of IL-6 on the fiber surface. Reprinted with permission from [220].

In comparison with the label-free technique, the fluorescent label technique suffers from inconveniences. It is necessary to pay attention to the potential loss of activity of the biomolecules as it is chemically conjugated with fluorescent tags. The performance of the fluorescence-based biosensor is mainly affected by the evanescent field intensity, fluorescent tags, and the number of bound antigens on the fiber surface. Hence the number of studies is not as high as for label-free biosensors in recent years. However, the better specific detection capability makes it more suitable for complex environments. Some important fluorescence-based fiber biosensors for protein dection are summerized in Table 5.

Table 5. Fluorescence-based fiber biosensors for protein detection.

Fiber Sensor Configuration	Detection Target	Functionalization Method	Sensitivity	Limit of Detection	Ref
Tapered fiber probe	serum protein	None	-	20 µg/mL	[213]
Tapered fiber probe	IL-6	Antibody based sandwich immunoassay	-	0.12 ng/mL	[214]
Fabry-Perot cavity	Rabbit IgG	Ag/Al	-	500 ng/mL	[216]
Unclad POF	Mouse IgG	Sandwich immunoassay + AuNPs	-	1 pg/mL	[25]
Unclad POF	AFP	Sandwich immunoassay + AuNPs	-	2 ng/mL	[217]
Unclad POF	SARS-CoV-2 N-protein	Sandwich immunoassay + AuNPs	-	1 pg/mL	[218]
Unclad fiber	IL-6	Au + sandwich immunoassay	-	1 pg/mL	[219]
Unclad fiber	IL-6	Biotin-SV coupling + sandwich immunoassay	-	0.1 pg/mL	[220]
Unclad POF	Mouse IgG	Sandwich immunoassay + liposome	-	2 pg/mL	[221]

3. Summary

As shown in Figure 17, fiber biosensor based on the above four sensing mechanisms have various structures, which possess their own advantages and disadvantages. In general, absorption- and fluorescence-based biosensors are usually labelled detection and are less susceptible to interference from non-specific binding, but the operation process is more cumbersome. Label-free biosensors based on phase-modulation are more widely used, and they have relatively higher sensitivity than intensity-modulated biosensors. Among them, SPR-based biosensors occupy a dominant position for their high sensitivity, simple fabrication, and real-time detection of biomolecular interactions. However, they not only require expensive equipment but also suffer instability issues. Although fiber grating-based sensors are not as sensitive as SPR sensors, they are more stable with temperature variation, and, due to their narrow signal bandwidth, it is possible to achieve multiplexing. Several methods have been developed to improve the sensitivity of grating fiber sensors. For FBG,

they can be combined with SPR to manufacture a sensor that is sensitive to external RI and can be temperature-compensated. It is worth mentioning that the inherent biocompatibility of FBG makes it a powerful tool in medical biosensors [222]. For LPG, MT and TAP can be used to significantly improve their sensitivity in aqueous solutions. The structural design of the interferometric sensor is the most flexible with a wide variety of forms. They also have high sensitivity and can be further improved by the Vernier effect. Scattering-based biosensors do not require additional reflective signal components, but they are limited by transmission loss, scattering efficiency, and signal collection efficiency.

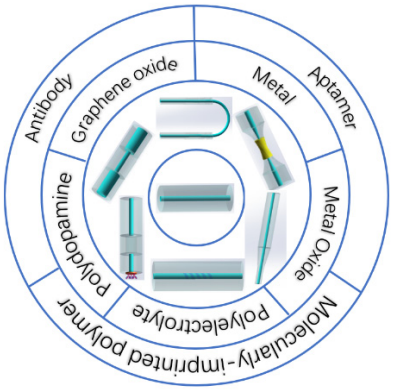

Figure 17. The structures of fiber biosensors and the modification methods.

4. Challenges and Opportunities

In this paper, we have introduced various types of protein recognition-based optical fiber biosensors, in terms of the principles of evanescent wave absorption, phase-modulation, scattering, and fluorescence, and summarized some applications for the detection of disease- and virus-related proteins. Recently, benefiting from the development of micromachining technology and modification technology, optical fibers have resulted in many advances in the field of biological sensing. Compared with other types of biosensors, optical fiber-based biosensors exhibit high sensitivity, low LoD, and good stability. Besides, they are relatively flexible in actual biological applications, since the optical fiber sensors based on the responses of external RI changes can detect different analytes only by adjusting the functional modified materials and the receptors. To date, the development of optical fiber sensors combined with microfluidics has been witnessed [59,223], which provides more benefits for the quantification and compactness of biological analyte detection.

However, there still many problems to address before actual commercial application. Mass production is hard to implement due to the fabrication complexity of the optical fiber biosensors. The precise and tedious biological modification processes are difficult to complete automatically by machine. Moreover, this also limits the repeatability and standardization of the biosensors.

Another serious issue is how to achieve practical application in vivo. At present, most of the protein detection is performed in biological fluids, such as serum or urine. The reason that biosensing still remains in the laboratory stage is the complexity and the difficulty of accessing real biological samples. More importantly, it is necessary to ensure that the optical fiber has enough stiffness to penetrate into soft tissue, which is a huge challenge for silica fibers with a diameter of only micrometers. Nevertheless, some researchers have been working on reducing the influence of individual differences in human serum [224] for the purpose of in vivo detection [153,225].

So as to break through the dilemma, researchers have been exploring the integration of optical fiber sensor devices with multichannel optofluidic platforms [226]. Optical microarray biosensors are powerful tools for the high-throughput analysis of multiple analytes in low sample volumes. However, another problem occurs, which is the lack of portability. Therefore, the future opportunities in research on optical fiber biosensors will

include studies on developing new integrated biosensors that are portable, easy to operate, capable of multiple automated analyses, and that have have good reproducibility.

In order to achieve commercialization, cost is an unavoidable issue. Although the optical fiber itself is cost-effective, some functional modification materials are expensive. As far as current interrogation systems is concerned, optical spectrum analyzers are complex and expensive [227]. The open challenge is to devolop the miniaturized interrogators and improve their performance. However, there have been some achievements that may promote the commercialization of optical fiber biosensors. On the one hand, the cost of optical fiber fabrication can be reduced by designing optical fiber structures that are easily standardized, such as a ball-resonator-interrogated optical backscatter reflectometer [228,229]. Moreover, Yang et al. demonstrated a cost effectively mass-produced technology, which plays a positive role in the promotion of marketization [230]. As for the optical interrogation, On the other hand, with the development of Internet of Things technology, the sensing platform of an integrated biochip makes the optical fiber biosensor more accessible [231]. It can be predicted that, after the above two challenges are further overcome, optical fiber biosensors will usher in explosive applications.

Author Contributions: Writing—original draft preparation, S.L.; writing—review and editing, Z.W.; supervision, X.S.; project administration, Q.W. All authors have read and agreed to the published version of the manuscript.

Funding: This research was funded by the National Natural Science Foundation of China for Excellent Young Scholars, grant number 62022016 and 11864025; National Natural Science Foundation of China, grant number 61835002, 61727817, 62021005; and National Key R&D Program of China from Ministry of Science and Technology, grant number 2019YFA0706300.

Institutional Review Board Statement: Not applicable.

Informed Consent Statement: Not applicable.

Data Availability Statement: Not applicable.

Conflicts of Interest: The authors declare no conflict of interest.

References

1. Von Heijne, G. The membrane protein universe: What's out there and why bother? *J. Intern. Med.* **2007**, *261*, 543–557. [CrossRef] [PubMed]
2. Edouard, S.; Jaafar, R.; Orain, N.; Parola, P.; Colson, P.; La Scola, B.; Fournier, P.-E.; Raoult, D.; Drancourt, M. Automated Western immunoblotting detection of anti-SARS-CoV-2 serum antibodies. *Eur. J. Clin. Microbiol. Infect. Dis.* **2021**, *40*, 1309–1317. [CrossRef] [PubMed]
3. Matos, L.L.d.; Trufelli, D.C.; de Matos, M.G.L.; da Silva Pinhal, M.A. Immunohistochemistry as an important tool in biomarkers detection and clinical practice. *Biomark. Insights* **2010**, *5*, 9–20. [CrossRef] [PubMed]
4. Finkelmeier, F.; Canli, Ö.; Tal, A.; Pleli, T.; Trojan, J.; Schmidt, M.; Kronenberger, B.; Zeuzem, S.; Piiper, A.; Greten, F.R.; et al. High levels of the soluble programmed death-ligand (sPD-L1) identify hepatocellular carcinoma patients with a poor prognosis. *Eur. J. Cancer* **2016**, *59*, 152–159. [CrossRef]
5. Joe, H.-E.; Yun, H.; Jo, S.-H.; Jun, M.B.G.; Min, B.-K. A review on optical fiber sensors for environmental monitoring. *Int. J. Precis. Eng. Manuf.-Green Technol.* **2018**, *5*, 173–191. [CrossRef]
6. Carrasco, S.; Benito-Peña, E.; Walt, D.R.; Moreno-Bondi, M.C. Fiber-optic array using molecularly imprinted microspheres for antibiotic analysis. *Chem. Sci.* **2015**, *6*, 3139–3147. [CrossRef]
7. Sun, D.; Fu, Y.; Yang, Y. Label-free detection of breast cancer biomarker using silica microfiber interferometry. *Opt. Commun.* **2020**, *463*, 125375. [CrossRef]
8. Arcadio, F.; Zeni, L.; Montemurro, D.; Eramo, C.; Di Ronza, S.; Perri, C.; D'Agostino, G.; Chiaretti, G.; Porto, G.; Cennamo, N. Biochemical sensing exploiting plasmonic sensors based on gold nanogratings and polymer optical fibers. *Photon. Res.* **2021**, *9*, 1397–1408. [CrossRef]
9. Vaiano, P.; Carotenuto, B.; Pisco, M.; Ricciardi, A.; Quero, G.; Consales, M.; Crescitelli, A.; Esposito, E.; Cusano, A. Lab on Fiber Technology for biological sensing applications. *Laser Photonics Rev.* **2016**, *10*, 922–961. [CrossRef]
10. Barozzi, M.; Manicardi, A.; Vannucci, A.; Candiani, A.; Sozzi, M.; Konstantaki, M.; Pissadakis, S.; Corradini, R.; Selleri, S.; Cucinotta, A. Optical Fiber Sensors for Label-Free DNA Detection. *J. Lightwave Technol.* **2017**, *35*, 3461–3472. [CrossRef]
11. Srivastava, S.K.; Arora, V.; Sapra, S.; Gupta, B.D. Localized Surface Plasmon Resonance-Based Fiber Optic U-Shaped Biosensor for the Detection of Blood Glucose. *Plasmonics* **2012**, *7*, 261–268. [CrossRef]

12. Cenci, L.; Andreetto, E.; Vestri, A.; Bovi, M.; Barozzi, M.; Iacob, E.; Busato, M.; Castagna, A.; Girelli, D.; Bossi, A.M. Surface plasmon resonance based on molecularly imprinted nanoparticles for the picomolar detection of the iron regulating hormone Hepcidin-25. *J. Nanobiotechnol.* **2015**, *13*, 51. [CrossRef] [PubMed]
13. Luo, B.; Wu, S.; Zhang, Z.; Zou, W.; Shi, S.; Zhao, M.; Zhong, N.; Liu, Y.; Zou, X.; Wang, L.; et al. Human heart failure biomarker immunosensor based on excessively tilted fiber gratings. *Biomed. Opt. Express* **2017**, *8*, 57–67. [CrossRef] [PubMed]
14. Kim, J.; Hong, S.C.; Hong, J.C.; Chang, C.L.; Park, T.J.; Kim, H.-J.; Lee, J. Clinical immunosensing of tuberculosis CFP-10 antigen in urine using interferometric optical fiber array. *Sens. Actuators B Chem.* **2015**, *216*, 184–191. [CrossRef]
15. Ohk, S.H.; Koo, O.K.; Sen, T.; Yamamoto, C.M.; Bhunia, A.K. Antibody–aptamer functionalized fibre-optic biosensor for specific detection of Listeria monocytogenes from food. *J. Appl. Microbiol.* **2010**, *109*, 808–817. [CrossRef]
16. Cennamo, N.; D'Agostino, G.; Perri, C.; Arcadio, F.; Chiaretti, G.; Parisio, E.M.; Camarlinghi, G.; Vettori, C.; Di Marzo, F.; Cennamo, R.; et al. Proof of Concept for a Quick and Highly Sensitive On-Site Detection of SARS-CoV-2 by Plasmonic Optical Fibers and Molecularly Imprinted Polymers. *Sensors* **2021**, *21*, 1681. [CrossRef]
17. Fan, X.; White, I.M.; Shopova, S.I.; Zhu, H.; Suter, J.D.; Sun, Y. Sensitive optical biosensors for unlabeled targets: A review. *Anal. Chim. Acta* **2008**, *620*, 8–26. [CrossRef]
18. Cooper, M. *Label-Free Biosensors: Techniques and Applications*; Cambridge University Press: Cambridge, UK, 2011. [CrossRef]
19. Liu, C.; Cai, Q.; Xu, B.; Zhu, W.; Zhang, L.; Zhao, J.; Chen, X. Graphene oxide functionalized long period grating for ultrasensitive label-free immunosensing. *Biosens. Bioelectron.* **2017**, *94*, 200–206. [CrossRef]
20. Sun, D.; Guo, T.; Ran, Y.; Huang, Y.; Guan, B.O. In-situ DNA hybridization detection with a reflective microfiber grating biosensor. *Biosens. Bioelectron.* **2014**, *61*, 541–546. [CrossRef]
21. Yu, W.; Lang, T.; Bian, J.; Kong, W. Label-free fiber optic biosensor based on thin-core modal interferometer. *Sens. Actuators B Chem.* **2016**, *228*, 322–329. [CrossRef]
22. Zhang, N.; Li, K.; Cui, Y.; Wu, Z.; Shum, P.P.; Auguste, J.-L.; Dinh, X.Q.; Humbert, G.; Wei, L. Ultra-sensitive chemical and biological analysis via specialty fibers with built-in microstructured optofluidic channels. *Lab A Chip* **2018**, *18*, 655–661. [CrossRef] [PubMed]
23. Sansone, L.; Macchia, E.; Taddei, C.; Torsi, L.; Giordano, M. Label-free optical biosensing at femtomolar detection limit. *Sens. Actuators B Chem.* **2018**, *255*, 1097–1104. [CrossRef]
24. Au-Soteropulos, C.E.; Au-Hunt, H.K. Attaching Biological Probes to Silica Optical Biosensors Using Silane Coupling Agents. *JoVE* **2012**, *63*, e3866. [CrossRef]
25. Hsieh, B.-Y.; Chang, Y.-F.; Ng, M.-Y.; Liu, W.-C.; Lin, C.-H.; Wu, H.-T.; Chou, C. Localized Surface Plasmon Coupled Fluorescence Fiber-Optic Biosensor with Gold Nanoparticles. *Anal. Chem.* **2007**, *79*, 3487–3493. [CrossRef]
26. Zubiate, P.; Zamarreño, C.R.; Sánchez, P.; Matias, I.R.; Arregui, F.J. High sensitive and selective C-reactive protein detection by means of lossy mode resonance based optical fiber devices. *Biosens. Bioelectron.* **2017**, *93*, 176–181. [CrossRef]
27. Shi, S.; Wang, L.; Su, R.; Liu, B.; Huang, R.; Qi, W.; He, Z. A polydopamine-modified optical fiber SPR biosensor using electroless-plated gold films for immunoassays. *Biosens. Bioelectron.* **2015**, *74*, 454–460. [CrossRef]
28. Caruso, F.; Niikura, K.; Furlong, D.N.; Okahata, Y. 2. Assembly of Alternating Polyelectrolyte and Protein Multilayer Films for Immunosensing. *Langmuir* **1997**, *13*, 3427–3433. [CrossRef]
29. Zhang, Y.; Shibru, H.; Cooper, K.L.; Wang, A. Miniature fiber-optic multicavity Fabry–Perot interferometric biosensor. *Opt. Lett.* **2005**, *30*, 1021–1023. [CrossRef]
30. Geim, A.K. Graphene: Status and prospects. *Science* **2009**, *324*, 1530–1534. [CrossRef]
31. Dash, J.N.; Jha, R. Temperature Insensitive PCF Interferometer Coated With Graphene Oxide Tip Sensor. *IEEE Photonics Technol. Lett.* **2016**, *28*, 1006–1009. [CrossRef]
32. Sridevi, S.; Vasu, K.S.; Jayaraman, N.; Asokan, S.; Sood, A.K. Optical bio-sensing devices based on etched fiber Bragg gratings coated with carbon nanotubes and graphene oxide along with a specific dendrimer. *Sens. Actuators B Chem.* **2014**, *195*, 150–155. [CrossRef]
33. Wang, Q.; Jing, J.; Wang, B. Highly Sensitive SPR Biosensor Based on Graphene Oxide and Staphylococcal Protein A Co-Modified TFBG for Human IgG Detection. *IEEE Trans. Instrum. Meas.* **2019**, *68*, 3350–3357. [CrossRef]
34. Narang, U.; Anderson, G.P.; Ligler, F.S.; Burans, J. Fiber optic-based biosensor for ricin. *Biosens. Bioelectron.* **1997**, *12*, 937–945. [CrossRef] [PubMed]
35. Shevchenko, Y.; Francis, T.J.; Blair, D.A.D.; Walsh, R.; DeRosa, M.C.; Albert, J. In Situ Biosensing with a Surface Plasmon Resonance Fiber Grating Aptasensor. *Anal. Chem.* **2011**, *83*, 7027–7034. [CrossRef]
36. Pathak, A.; Parveen, S.; Gupta, B.D. Ultrasensitive, highly selective, and real-time detection of protein using functionalized CNTs as MIP platform for FOSPR-based biosensor. *Nanotechnology* **2017**, *28*, 355503. [CrossRef]
37. Litman, G.W.; Rast, J.P.; Shamblott, M.J.; Haire, R.N.; Hulst, M.; Roess, W.; Litman, R.T.; Hinds-Frey, K.R.; Zilch, A.; Amemiya, C.T. Phylogenetic diversification of immunoglobulin genes and the antibody repertoire. *Mol. Biol. Evol.* **1993**, *10*, 60–72. [CrossRef]
38. Joshi, R.; Janagama, H.; Dwivedi, H.P.; Senthil Kumar, T.M.A.; Jaykus, L.-A.; Schefers, J.; Sreevatsan, S. Selection, characterization, and application of DNA aptamers for the capture and detection of Salmonella enterica serovars. *Mol. Cell. Probes* **2009**, *23*, 20–28. [CrossRef]
39. Iliuk, A.B.; Hu, L.; Tao, W.A. Aptamer in Bioanalytical Applications. *Anal. Chem.* **2011**, *83*, 4440–4452. [CrossRef]
40. Song, K.-M.; Lee, S.; Ban, C. Aptamers and Their Biological Applications. *Sensors* **2012**, *12*, 612–631. [CrossRef]

41. Haupt, K.; Medina Rangel, P.X.; Bui, B.T.S. Molecularly Imprinted Polymers: Antibody Mimics for Bioimaging and Therapy. *Chem. Rev.* **2020**, *120*, 9554–9582. [CrossRef]
42. Scriba, G.K.E. Chiral recognition in separation science—An update. *J. Chromatogr. A* **2016**, *1467*, 56–78. [CrossRef] [PubMed]
43. Li, W.; Zhang, Q.; Wang, Y.; Ma, Y.; Guo, Z.; Liu, Z. Controllably Prepared Aptamer–Molecularly Imprinted Polymer Hybrid for High-Specificity and High-Affinity Recognition of Target Proteins. *Anal. Chem.* **2019**, *91*, 4831–4837. [CrossRef] [PubMed]
44. Marques, L.; Hernandez, F.U.; James, S.W.; Morgan, S.P.; Clark, M.; Tatam, R.P.; Korposh, S. Highly sensitive optical fibre long period grating biosensor anchored with silica core gold shell nanoparticles. *Biosens. Bioelectron.* **2016**, *75*, 222–231. [CrossRef] [PubMed]
45. Wu, Q.; Semenova, Y.; Wang, P.; Farrell, G. High sensitivity SMS fiber structure based refractometer—Analysis and experiment. *Opt. Express* **2011**, *19*, 7937–7944. [CrossRef] [PubMed]
46. Rifat, A.A.; Mahdiraji, G.A.; Sua, Y.M.; Ahmed, R.; Shee, Y.G.; Adikan, F.R.M. Highly sensitive multi-core flat fiber surface plasmon resonance refractive index sensor. *Opt. Express* **2016**, *24*, 2485–2495. [CrossRef] [PubMed]
47. Gangwar, R.K.; Singh, V.K. Highly Sensitive Surface Plasmon Resonance Based D-Shaped Photonic Crystal Fiber Refractive Index Sensor. *Plasmonics* **2017**, *12*, 1367–1372. [CrossRef]
48. Xu, Z.; Sun, Q.; Li, B.; Luo, Y.; Lu, W.; Liu, D.; Shum, P.P.; Zhang, L. Highly sensitive refractive index sensor based on cascaded microfiber knots with Vernier effect. *Opt. Express* **2015**, *23*, 6662–6672. [CrossRef]
49. De Acha, N.; Socorro-Leránoz, A.B.; Elosúa, C.; Matías, I.R. Trends in the Design of Intensity-Based Optical Fiber Biosensors (2010–2020). *Biosensors* **2021**, *11*, 197. [CrossRef]
50. Leung, A.; Shankar, P.M.; Mutharasan, R. A review of fiber-optic biosensors. *Sens. Actuators B Chem.* **2007**, *125*, 688–703. [CrossRef]
51. Sai, V.V.R.; Kundu, T.; Deshmukh, C.; Titus, S.; Kumar, P.; Mukherji, S. Label-free fiber optic biosensor based on evanescent wave absorbance at 280 nm. *Sens. Actuators B Chem.* **2010**, *143*, 724–730. [CrossRef]
52. Leung, A.; Shankar, P.; Mutharasan, R. Real-time monitoring of bovine serum albumin at femtogram/ml levels on antibody-immobilized tapered fibers. *Sens. Actuators B-Chem.* **2007**, *123*, 888–895. [CrossRef]
53. Petropoulou, A.; Gibson, T.J.; Themistou, E.; Pispas, S.; Riziotis, C. Development of amphiphilic block copolymers as silica optical fiber overlayers for BSA protein detection. *Mater. Chem. Phys.* **2018**, *216*, 421–428. [CrossRef]
54. Li, K.; Liu, G.; Wu, Y.; Hao, P.; Zhou, W.; Zhang, Z. Gold nanoparticle amplified optical microfiber evanescent wave absorption biosensor for cancer biomarker detection in serum. *Talanta* **2014**, *120*, 419–424. [CrossRef] [PubMed]
55. Ramakrishna, B.; Sai, V.V.R. Evanescent wave absorbance based U-bent fiber probe for immunobiosensor with gold nanoparticle labels. *Sens. Actuators B Chem.* **2016**, *226*, 184–190. [CrossRef]
56. Bandaru, R.; Divagar, M.; Khanna, S.; Danny, C.G.; Gupta, S.; Janakiraman, V.; Sai, V.V.R. U-bent fiber optic plasmonic biosensor platform for ultrasensitive analyte detection. *Sens. Actuators B Chem.* **2020**, *321*, 128463. [CrossRef]
57. Chiang, C.-Y.; Huang, T.-T.; Wang, C.-H.; Huang, C.-J.; Tsai, T.-H.; Yu, S.-N.; Chen, Y.-T.; Hong, S.-W.; Hsu, C.-W.; Chang, T.-C.; et al. Fiber optic nanogold-linked immunosorbent assay for rapid detection of procalcitonin at femtomolar concentration level. *Biosens. Bioelectron.* **2020**, *151*, 111871. [CrossRef]
58. Divagar, M.; Gayathri, R.; Rasool, R.; Shamlee, J.K.; Bhatia, H.; Satija, J.; Sai, V.V.R. Plasmonic Fiberoptic Absorbance Biosensor (P-FAB) for Rapid Detection of SARS-CoV-2 Nucleocapsid Protein. *IEEE Sens. J.* **2021**, *21*, 22758–22766. [CrossRef]
59. Xu, W.; Zhuo, Y.; Song, D.; Han, X.; Xu, J.; Long, F. Development of a novel label-free all-fiber optofluidic biosensor based on Fresnel reflection and its applications. *Anal. Chim. Acta* **2021**, *1181*, 338910. [CrossRef]
60. Guo, X. Surface plasmon resonance based biosensor technique: A review. *J. Biophotonics* **2012**, *5*, 483–501. [CrossRef]
61. Homola, J.; Yee, S.S.; Gauglitz, G. Surface plasmon resonance sensors: Review. *Sens. Actuators B Chem.* **1999**, *54*, 3–15. [CrossRef]
62. Fu, H.; Zhang, S.; Chen, H.; Weng, J. Graphene Enhances the Sensitivity of Fiber-Optic Surface Plasmon Resonance Biosensor. *IEEE Sens. J.* **2015**, *15*, 5478–5482. [CrossRef]
63. Urrutia, A.; Bojan, K.; Marques, L.; Mullaney, K.; Goicoechea, J.; James, S.; Clark, M.; Tatam, R.; Korposh, S. Novel Highly Sensitive Protein Sensors Based on Tapered Optical Fibres Modified with Au-Based Nanocoatings. *J. Sens.* **2016**, *2016*, 8129387. [CrossRef]
64. Cennamo, N.; Pasquardini, L.; Arcadio, F.; Lunelli, L.; Vanzetti, L.; Carafa, V.; Altucci, L.; Zeni, L. SARS-CoV-2 spike protein detection through a plasmonic D-shaped plastic optical fiber aptasensor. *Talanta* **2021**, *233*, 122532. [CrossRef] [PubMed]
65. Sai, V.V.R.; Kundu, T.; Mukherji, S. Novel U-bent fiber optic probe for localized surface plasmon resonance based biosensor. *Biosens. Bioelectron.* **2009**, *24*, 2804–2809. [CrossRef]
66. Tyagi, D.; Mishra, S.K.; Zou, B.; Lin, C.; Hao, T.; Zhang, G.; Lu, A.; Chiang, K.S.; Yang, Z. Nano-functionalized long-period fiber grating probe for disease-specific protein detection. *J. Mater. Chem. B* **2018**, *6*, 386–392. [CrossRef]
67. Jiang, Q.; Xue, M.; Liang, P.; Zhang, C.; Lin, J.; Ouyang, J. Principle and experiment of protein detection based on optical fiber sensing. *Photonic Sens.* **2017**, *7*, 317–324. [CrossRef]
68. Briand, E.; Salmain, M.; Herry, J.-M.; Perrot, H.; Compère, C.; Pradier, C.-M. Building of an immunosensor: How can the composition and structure of the thiol attachment layer affect the immunosensor efficiency? *Biosens. Bioelectron.* **2006**, *22*, 440–448. [CrossRef]
69. Briand, E.; Salmain, M.; Compere, C.; Pradier, C.-M. Immobilization of Protein A on SAMS for the elaboration of immunosensors. *Colloids Surf. B Biointerfaces* **2007**, *53*, 215–224. [CrossRef]

70. Ko, S.; Park, T.J.; Kim, H.-S.; Kim, J.-H.; Cho, Y.-J. Directed self-assembly of gold binding polypeptide-protein A fusion proteins for development of gold nanoparticle-based SPR immunosensors. *Biosens. Bioelectron.* **2009**, *24*, 2592–2597. [CrossRef]
71. Wong, W.C.; Chan, C.C.; Boo, J.L.; Teo, Z.Y.; Tou, Z.Q.; Yang, H.B.; Li, C.M.; Leong, K.C. Photonic Crystal Fiber Surface Plasmon Resonance Biosensor Based on Protein G Immobilization. *IEEE J. Sel. Top. Quantum Electron.* **2013**, *19*, 4602107. [CrossRef]
72. Sharma, A.K.; Gupta, B.D. On the sensitivity and signal to noise ratio of a step-index fiber optic surface plasmon resonance sensor with bimetallic layers. *Opt. Commun.* **2005**, *245*, 159–169. [CrossRef]
73. Kravets, V.G.; Jalil, R.; Kim, Y.J.; Ansell, D.; Aznakayeva, D.E.; Thackray, B.; Britnell, L.; Belle, B.D.; Withers, F.; Radko, I.P.; et al. Graphene-protected copper and silver plasmonics. *Sci. Rep.* **2014**, *4*, 5517. [CrossRef] [PubMed]
74. Wang, Q.; Wang, B.-T. Surface plasmon resonance biosensor based on graphene oxide/silver coated polymer cladding silica fiber. *Sens. Actuators B Chem.* **2018**, *275*, 332–338. [CrossRef]
75. Bao, Q.; Zhang, H.; Yang, J.-x.; Wang, S.; Tang, D.Y.; Jose, R.; Ramakrishna, S.; Lim, C.T.; Loh, K.P. Graphene–Polymer Nanofiber Membrane for Ultrafast Photonics. *Adv. Funct. Mater.* **2010**, *20*, 782–791. [CrossRef]
76. Cao, J.; Sun, T.; Grattan, K.T.V. Gold nanorod-based localized surface plasmon resonance biosensors: A review. *Sens. Actuators B Chem.* **2014**, *195*, 332–351. [CrossRef]
77. Willets, K.A.; Van Duyne, R.P. Localized Surface Plasmon Resonance Spectroscopy and Sensing. *Annu. Rev. Phys. Chem.* **2007**, *58*, 267–297. [CrossRef]
78. Mayer, K.M.; Hafner, J.H. Localized Surface Plasmon Resonance Sensors. *Chem. Rev.* **2011**, *111*, 3828–3857. [CrossRef]
79. Nguyen, T.H.; Hardwick, S.A.; Sun, T.; Grattan, K.T.V. Intrinsic Fluorescence-Based Optical Fiber Sensor for Cocaine Using a Molecularly Imprinted Polymer as the Recognition Element. *IEEE Sens. J.* **2012**, *12*, 255–260. [CrossRef]
80. Sanders, M.; Lin, Y.; Bono, T.; Lindquist, R. An enhanced LSPR fiber-optic nanoprobe for ultrasensitive detection of protein biomarkers. *Biosens. Bioelectron.* **2014**, *61C*, 95–101. [CrossRef]
81. Lépinay, S.; Nause, A.; Ianoul, A.; Albert, J. Improved detection limits of protein optical fiber biosensors coated with gold nanoparticles. *Biosens. Bioelectron.* **2013**, *52C*, 337–344. [CrossRef]
82. Lu, M.; Zhu, H.; Bazuin, C.G.; Peng, W.; Masson, J.-F. Polymer-Templated Gold Nanoparticles on Optical Fibers for Enhanced-Sensitivity Localized Surface Plasmon Resonance Biosensors. *ACS Sens.* **2019**, *4*, 613–622. [CrossRef] [PubMed]
83. Kim, H.-M.; Uh, M.; Jeong, D.H.; Lee, H.-Y.; Park, J.-H.; Lee, S.-K. Localized surface plasmon resonance biosensor using nanopatterned gold particles on the surface of an optical fiber. *Sens. Actuators B Chem.* **2019**, *280*, 183–191. [CrossRef]
84. Yang, C.-T.; Wu, L.; Bai, P.; Thierry, B. Investigation of plasmonic signal enhancement based on long range surface plasmon resonance with gold nanoparticle tags. *J. Mater. Chem. C* **2016**, *4*, 9897–9904. [CrossRef]
85. Chen, X.; Bu, W.; Wu, Z.; Zhang, H.; Shum, P.P.; Shao, X.; Pu, J. Near-infrared long-range surface plasmon resonance in a D-shaped honeycomb microstructured optical fiber coated with Au film. *Opt. Express* **2021**, *29*, 16455–16468. [CrossRef]
86. Cheng, Z.; Wang, Q.; Zhu, A.-s.; Qiu, F.-m.; Niu, L.-Y.; Jing, J.-Y. Au-nanoshells modified surface field enhanced LRSPR biosensor with low LOD for highly sensitive hIgG sensing. *Opt. Laser Technol.* **2021**, *134*, 106656. [CrossRef]
87. Jing, J.; Liu, K.; Jiang, J.; Xu, T.; Wang, S.; Ma, J.; Zhang, Z.; Zhang, W.; Liu, T. Double-Antibody Sandwich Immunoassay and Plasmonic Coupling Synergistically Improved Long-Range SPR Biosensor with Low Detection Limit. *Nanomaterials* **2021**, *11*, 2137. [CrossRef]
88. Yang, F.; Sambles, J.R. Determination of the optical permittivity and thickness of absorbing films using long range modes. *J. Mod. Opt.* **1997**, *44*, 1155–1163. [CrossRef]
89. Marciniak, M.; Grzegorzewski, J.; Szustakowski, M. Analysis of lossy mode cut-off conditions in planar waveguides with semiconductor guiding layer. *IEE Proc. J Optoelectron.* **1993**, *140*, 247–252. [CrossRef]
90. Villar, I.D.; Zamarreno, C.R.; Hernaez, M.; Arregui, F.J.; Matias, I.R. Lossy Mode Resonance Generation With Indium-Tin-Oxide-Coated Optical Fibers for Sensing Applications. *J. Lightwave Technol.* **2010**, *28*, 111–117. [CrossRef]
91. Sanchez, P.; Zamarreno, C.R.; Hernaez, M.; Villar, I.D.; Matias, I.R.; Arregui, F.J. Considerations for Lossy-Mode Resonance-Based Optical Fiber Sensor. *IEEE Sens. J.* **2013**, *13*, 1167–1171. [CrossRef]
92. Sanchez, P.; Zamarreño, C.R.; Hernaez, M.; Del Villar, I.; Fernandez-Valdivielso, C.; Matias, I.R.; Arregui, F.J. Lossy mode resonances toward the fabrication of optical fiber humidity sensors. *Meas. Sci. Technol.* **2011**, *23*, 014002. [CrossRef]
93. Villar, I.D.; Torres, V.; Beruete, M. Experimental demonstration of lossy mode and surface plasmon resonance generation with Kretschmann configuration. *Opt. Lett.* **2015**, *40*, 4739–4742. [CrossRef] [PubMed]
94. Sanchez, P.; Zamarreño, C.R.; Hernaez, M.; Matias, I.R.; Arregui, F.J. Optical fiber refractometers based on Lossy Mode Resonances by means of SnO2 sputtered coatings. *Sens. Actuators B Chem.* **2014**, *202*, 154–159. [CrossRef]
95. Wang, Q.; Zhao, W.-M. A comprehensive review of lossy mode resonance-based fiber optic sensors. *Opt. Lasers Eng.* **2018**, *100*, 47–60. [CrossRef]
96. Socorro, A.B.; Corres, J.M.; Del Villar, I.; Arregui, F.J.; Matias, I.R. Fiber-optic biosensor based on lossy mode resonances. *Sens. Actuators B Chem.* **2012**, *174*, 263–269. [CrossRef]
97. Socorro, A.B.; Del Villar, I.; Corres, J.M.; Arregui, F.J.; Matias, I.R. Spectral width reduction in lossy mode resonance-based sensors by means of tapered optical fibre structures. *Sens. Actuators B Chem.* **2014**, *200*, 53–60. [CrossRef]
98. Vicente, A.; Santano, D.; Zubiate, P.; Urrutia, A.; Del Villar, I.; Zamarreño, C.R. Lossy mode resonance sensors based on nanocoated multimode-coreless-multimode fibre. *Sens. Actuators B Chem.* **2020**, *304*, 126955. [CrossRef]

99. Wang, B.-T.; Wang, Q. An interferometric optical fiber biosensor with high sensitivity for IgG/anti-IgG immunosensing. *Opt. Commun.* **2018**, *426*, 388–394. [CrossRef]
100. Wu, J.; Wang, Q.; Song, B.; Zhang, C.; Liu, B.; Lin, W.; Duan, S.; Bai, H. Label-Free Biosensor Based on Coreless-Fiber-Coupled Microcavity for Protein Detection. *IEEE Photonics Technol. Lett.* **2021**, *33*, 495–498. [CrossRef]
101. Li, Z.; Liao, C.; Chen, D.; Song, J.; Jin, W.; Peng, G.-D.; Zhu, F.; Wang, Y.; He, J.; Wang, Y. Label-free detection of bovine serum albumin based on an in-fiber Mach-Zehnder interferometric biosensor. *Opt. Express* **2017**, *25*, 17105–17113. [CrossRef]
102. Janik, M.; Koba, M.; Celebańska, A.; Bock, W.J.; Śmietana, M. Live *E. coli* bacteria label-free sensing using a microcavity in-line Mach-Zehnder interferometer. *Sci. Rep.* **2018**, *8*, 17176. [CrossRef] [PubMed]
103. Liu, H.; Sun, Y.; Guo, J.; Liu, W.; Liu, L.; Meng, Y.; Yu, X. Temperature-Insensitive Label-Free Sensors for Human IgG Based on S-Tapered Optical Fiber Sensors. *IEEE Access* **2021**, *9*, 116286–116293. [CrossRef]
104. Yang, X.; Yu, W.; Liu, Z.; Yang, J.; Zhang, Y.; Kong, D.; Long, Q.; Yuan, T.; Cao, J.; Yuan, L.; et al. Optofluidic twin-core hollow fiber interferometer for label-free sensing of the streptavidin-biotin binding. *Sens. Actuators B Chem.* **2018**, *277*, 353–359. [CrossRef]
105. Li, Y.; Ma, H.; Gan, L.; Gong, A.; Zhang, H.; Liu, D.; Sun, Q. Selective and sensitive *Escherichia coli* detection based on a T4 bacteriophage-immobilized multimode microfiber. *J. Biophotonics* **2018**, *11*, e201800012. [CrossRef]
106. Sun, D.; Sun, L.; Guo, T.; Guan, B. Label-Free Thrombin Detection Using a Tapered Fiber-Optic Interferometric Aptasensor. *J. Lightwave Technol.* **2019**, *37*, 2756–2761. [CrossRef]
107. Liu, X.; Lin, W.; Xiao, P.; Yang, M.; Sun, L.-P.; Zhang, Y.; Xue, W.; Guan, B.-O. Polydopamine-based molecular imprinted optic microfiber sensor enhanced by template-mediated molecular rearrangement for ultra-sensitive C-reactive protein detection. *Chem. Eng. J.* **2020**, *387*, 124074. [CrossRef]
108. Ravikumar, R.; Chen, L.; Jayaraman, P.; Poh, C.L.; Chan, C. Chitosan-nickel film based interferometric optical fiber sensor for label-free detection of histidine tagged proteins. *Biosens. Bioelectron.* **2017**, *99*, 578–585. [CrossRef]
109. Antonio-Lopez, J.E.; Castillo-Guzman, A.; May-Arrioja, D.A.; Selvas-Aguilar, R.; LiKamWa, P. Tunable multimode-interference bandpass fiber filter. *Opt. Lett.* **2010**, *35*, 324–326. [CrossRef]
110. Huong, V.T.; Van Tran, V.; Lee, N.Y.; Van Hoang, D.; Loan Trinh, K.T.; Phan, T.B.; Thi Tran, N.H. Bimetallic Thin-Film Combination of Surface Plasmon Resonance-Based Optical Fiber Cladding with the Polarizing Homodyne Balanced Detection Method and Biomedical Assay Application. *Langmuir* **2020**, *36*, 9967–9976. [CrossRef]
111. Li, X.; Chen, N.; Zhou, X.; Gong, P.; Wang, S.; Zhang, Y.; Zhao, Y. A review of specialty fiber biosensors based on interferometer configuration. *J. Biophotonics* **2021**, *14*, e202100068. [CrossRef]
112. Yang, J.; Sandhu, P.; Liang, W.; Xu, C.; Li, Y. Label-Free Fiber Optic Biosensors with Enhanced Sensitivity. *IEEE J. Sel. Top. Quantum Electron.* **2007**, *13*, 1691–1696. [CrossRef]
113. Chen, L.; Chan, C.C.; Ni, K.; Hu, P.; Li, T.; Wong, W.C.; Balamurali, P.; Menon, R.; Shaillender, M.; Neu, B.; et al. Label-free fiber-optic interferometric immunosensors based on waist-enlarged fusion taper. *Sens. Actuators B Chem.* **2013**, *178*, 176–184. [CrossRef]
114. Wysokiński, K.; Budnicki, D.; Fidelus, J.; Szostkiewicz, Ł.; Ostrowski, Ł.; Murawski, M.; Staniszewski, M.; Staniszewska, M.; Napierała, M.; Nasiłowski, T. Dual-core all-fiber integrated immunosensor for detection of protein antigens. *Biosens. Bioelectron.* **2018**, *114*, 22–29. [CrossRef] [PubMed]
115. Wang, Q.; Liu, X.; Xia, J.; Zhao, Y. A Novel Long-Tail Fiber Current Sensor Based on Fiber Loop Ring-Down Spectroscopy and Fabry-Perot Cavity Filled With Magnetic Fluid. *IEEE Trans. Instrum. Meas.* **2015**, *64*, 2005–2011. [CrossRef]
116. Petuchowski, S.; Giallorenzi, T.; Sheem, S. A sensitive fiber-optic Fabry-Perot interferometer. *IEEE J. Quantum Electron.* **1981**, *17*, 2168–2170. [CrossRef]
117. Chen, L.H.; Ang, X.M.; Chan, C.C.; Shaillender, M.; Neu, B.; Wong, W.C.; Zu, P.; Leong, K.C. Layer-By-Layer (Chitosan/Polystyrene Sulfonate) Membrane-Based Fabry–Perot Interferometric Fiber Optic Biosensor. *IEEE J. Sel. Top. Quantum Electron.* **2012**, *18*, 1457–1464. [CrossRef]
118. Chen, L.H.; Chan, C.C.; Menon, R.; Balamurali, P.; Wong, W.C.; Ang, X.M.; Hu, P.B.; Shaillender, M.; Neu, B.; Zu, P.; et al. Fabry–Perot fiber-optic immunosensor based on suspended layer-by-layer (chitosan/polystyrene sulfonate) membrane. *Sens. Actuators B Chem.* **2013**, *188*, 185–192. [CrossRef]
119. Liu, X.; Jiang, M.; Dong, T.; Sui, Q.; Geng, X. Label-Free Immunosensor Based on Optical Fiber Fabry–Perot Interferometer. *IEEE Sens. J.* **2016**, *16*, 7515–7520. [CrossRef]
120. Xie, L.; Nguyen, L.V.; Ebendorff-Heidepriem, H.; Warren-Smith, S. Multiplexed Optical Fiber Biochemical Sensing Using Cascaded C-Shaped Fabry–Perot Interferometers. *IEEE Sens. J.* **2019**, *19*, 10425–10431. [CrossRef]
121. Chunyang, H.; Hui, D.; Xianli, L.; Shaofei, D. Temperature insensitive refractive index sensor based on single-mode micro-fiber Sagnac loop interferometer. *Appl. Phys. Lett.* **2014**, *104*, 181906. [CrossRef]
122. Gao, S.; Sun, L.-P.; Li, J.; Jin, L.; Ran, Y.; Huang, Y.; Guan, B.-O. High-sensitivity DNA biosensor based on microfiber Sagnac interferometer. *Opt. Express* **2017**, *25*, 13305–13313. [CrossRef]
123. Wang, X.-Z.; Wang, Q. A High-Birefringence Microfiber Sagnac-Interferometer Biosensor Based on the Vernier Effect. *Sensors* **2018**, *18*, 4114. [CrossRef] [PubMed]
124. Li, X.; Nguyen, L.V.; Zhao, Y.; Ebendorff-Heidepriem, H.; Warren-Smith, S.C. High-sensitivity Sagnac-interferometer biosensor based on exposed core microstructured optical fiber. *Sens. Actuators B Chem.* **2018**, *269*, 103–109. [CrossRef]

125. Szu-Wen, Y.; Tzong-Lin, W.; Cheng Wen, W.; Hung-Chun, C. Numerical modeling of weakly fused fiber-optic polarization beamsplitters. Part II: The three-dimensional electromagnetic model. *J. Lightwave Technol.* **1998**, *16*, 691–696. [CrossRef]
126. Tazawa, H.; Kanie, T.; Katayama, M. Fiber-optic coupler based refractive index sensor and its application to biosensing. *Appl. Phys. Lett.* **2007**, *91*, 113901. [CrossRef]
127. Bo, L.; O'Mahony, C.C.; Semenova, Y.; Gilmartin, N.; Wang, P.; Farrell, G. Microfiber coupler based label-free immunosensor. *Opt. Express* **2014**, *22*, 8150–8155. [CrossRef]
128. Zhou, W.; Li, K.; Wei, Y.; Hao, P.; Chi, M.; Liu, Y.; Wu, Y. Ultrasensitive label-free optical microfiber coupler biosensor for detection of cardiac troponin I based on interference turning point effect. *Biosens. Bioelectron.* **2018**, *106*, 99–104. [CrossRef]
129. Li, K.; Zhang, N.; Ying Zhang, N.M.; Zhou, W.; Zhang, T.; Chen, M.; Wei, L. Birefringence induced Vernier effect in optical fiber modal interferometers for enhanced sensing. *Sens. Actuators B Chem.* **2018**, *275*, 16–24. [CrossRef]
130. Chen, L.; Leng, Y.-K.; Liu, B.; Liu, J.; Wan, S.-P.; Wu, T.; Yuan, J.; Shao, L.; Gu, G.; Fu, Y.Q.; et al. Ultrahigh-sensitivity label-free optical fiber biosensor based on a tapered singlemode- no core-singlemode coupler for Staphylococcus aureus detection. *Sens. Actuators B Chem.* **2020**, *320*, 128283. [CrossRef]
131. Fang, X.; Zhang, W.; Li, J.; Lin, C.; Chen, Z.; Zhang, M.; Huang, S.; Lu, D.; Wan, M.; Qiu, X. Signal processing assisted Vernier effect in a single interferometer for sensitivity magnification. *Opt. Express* **2021**, *29*, 11570–11581. [CrossRef]
132. Hill, K.O.; Fujii, Y.; Johnson, D.C.; Kawasaki, B.S. Photosensitivity in optical fiber waveguides: Application to reflection filter fabrication. *Appl. Phys. Lett.* **1978**, *32*, 647–649. [CrossRef]
133. Hill, K.O.; Meltz, G. Fiber Bragg grating technology fundamentals and overview. *J. Lightwave Technol.* **1997**, *15*, 1263–1276. [CrossRef]
134. Kersey, A.D.; Davis, M.A.; Patrick, H.J.; LeBlanc, M.; Koo, K.P.; Askins, C.G.; Putnam, M.A.; Friebele, E.J. Fiber grating sensors. *J. Lightwave Technol.* **1997**, *15*, 1442–1463. [CrossRef]
135. Srinivasan, R.; Umesh, S.; Murali, S.; Asokan, S.; Siva Gorthi, S. Bare fiber Bragg grating immunosensor for real-time detection of Escherichia coli bacteria. *J. Biophotonics* **2017**, *10*, 224–230. [CrossRef]
136. Shivananju, B.N.; Renilkumar, M.; Prashanth, G.R.; Asokan, S.; Varma, M.M. Detection Limit of Etched Fiber Bragg Grating Sensors. *J. Lightwave Technol.* **2013**, *31*, 2441–2447. [CrossRef]
137. Tsigaridas, G.; Polyzos, D.; Ioannou, A.; Fakis, M.; Persephonis, P. Theoretical and experimental study of refractive index sensors based on etched fiber Bragg gratings. *Sens. Actuators A Phys.* **2014**, *209*, 9–15. [CrossRef]
138. Sridevi, S.; Vasu, K.S.; Asokan, S.; Sood, A.K. Sensitive detection of C-reactive protein using optical fiber Bragg gratings. *Biosens. Bioelectron.* **2015**, *65*, 251–256. [CrossRef]
139. Bekmurzayeva, A.; Dukenbayev, K.; Shaimerdenova, M.; Bekniyazov, I.; Ayupova, T.; Sypabekova, M.; Molardi, C.; Tosi, D. Etched Fiber Bragg Grating Biosensor Functionalized with Aptamers for Detection of Thrombin. *Sensors* **2018**, *18*, 4298. [CrossRef]
140. Schulze, S.; Wehrhold, M.; Hille, C. Femtosecond-Pulsed Laser Written and Etched Fiber Bragg Gratings for Fiber-Optical Biosensing. *Sensors* **2018**, *18*, 2844. [CrossRef]
141. Martinez, A.; Dubov, M.; Khrushchev, I.; Bennion, I. Direct writing of fibre Bragg gratings by femtosecond laser. *Electron. Lett.* **2004**, *40*, 1170–1172. [CrossRef]
142. He, J.; Xu, B.; Xu, X.; Liao, C.; Wang, Y. Review of Femtosecond-Laser-Inscribed Fiber Bragg Gratings: Fabrication Technologies and Sensing Applications. *Photonic Sens.* **2021**, *11*, 203–226. [CrossRef]
143. Albert, J.; Shao, L.-Y.; Caucheteur, C. Tilted fiber Bragg grating sensors. *Laser Photonics Rev.* **2013**, *7*, 83–108. [CrossRef]
144. Shevchenko, Y.Y.; Albert, J. Plasmon resonances in gold-coated tilted fiber Bragg gratings. *Opt. Lett.* **2007**, *32*, 211–213. [CrossRef]
145. Phan Huy, M.C.; Laffont, G.; Dewynter, V.; Ferdinand, P.; Labonté, L.; Pagnoux, D.; Roy, P.; Blanc, W.; Dussardier, B. Tilted Fiber Bragg Grating photowritten in microstructured optical fiber for improved refractive index measurement. *Opt. Express* **2006**, *14*, 10359–10370. [CrossRef] [PubMed]
146. Maguis, S.; Laffont, G.; Ferdinand, P.; Carbonnier, B.; Kham, K.; Mekhalif, T.; Millot, M.-C. Biofunctionalized tilted Fiber Bragg Gratings for label-free immunosensing. *Opt. Express* **2008**, *16*, 19049–19062. [CrossRef]
147. Luo, B.; Wu, S.; Zou, W.; Zhang, Z.; Zhao, M.; Shi, S.; Liu, Y.; Xi, X.; Zeng, Z.; Liang, W.; et al. Label-free immunoassay for porcine circovirus type 2 based on excessively tilted fiber grating modified with staphylococcal protein A. *Biosens. Bioelectron.* **2016**, *86*, 1054–1060. [CrossRef] [PubMed]
148. Sun, Y.; Guo, X.; Moreno, Y.; Sun, Q.; Yan, Z.; Zhang, L. Sensitivity adjustable biosensor based on graphene oxide coated excessively tilted fiber grating. *Sens. Actuators B Chem.* **2022**, *351*, 130832. [CrossRef]
149. Voisin, V.; Pilate, J.; Damman, P.; Mégret, P.; Caucheteur, C. Highly sensitive detection of molecular interactions with plasmonic optical fiber grating sensors. *Biosens. Bioelectron.* **2014**, *51*, 249–254. [CrossRef]
150. Ribaut, C.; Voisin, V.; Malachovská, V.; Dubois, V.; Mégret, P.; Wattiez, R.; Caucheteur, C. Small biomolecule immunosensing with plasmonic optical fiber grating sensor. *Biosens. Bioelectron.* **2016**, *77*, 315–322. [CrossRef]
151. Guo, T.; Liu, F.; Liang, X.; Qiu, X.; Huang, Y.; Xie, C.; Xu, P.; Mao, W.; Guan, B.-O.; Albert, J. Highly sensitive detection of urinary protein variations using tilted fiber grating sensors with plasmonic nanocoatings. *Biosens. Bioelectron.* **2016**, *78*, 221–228. [CrossRef]
152. Han, L.; Guo, T.; Xie, C.; Xu, P.; Lao, J.; Zhang, X.; Xu, J.; Chen, X.; Huang, Y.; Liang, X.; et al. Specific Detection of Aquaporin-2 Using Plasmonic Tilted Fiber Grating Sensors. *J. Lightwave Technol.* **2017**, *35*, 3360–3365. [CrossRef]

153. Ribaut, C.; Loyez, M.; Larrieu, J.-C.; Chevineau, S.; Lambert, P.; Remmelink, M.; Wattiez, R.; Caucheteur, C. Cancer biomarker sensing using packaged plasmonic optical fiber gratings: Towards in vivo diagnosis. *Biosens. Bioelectron.* **2017**, *92*, 449–456. [CrossRef] [PubMed]
154. Lobry, M.; Loyez, M.; Chah, K.; Hassan, E.M.; Goormaghtigh, E.; DeRosa, M.C.; Wattiez, R.; Caucheteur, C. HER2 biosensing through SPR-envelope tracking in plasmonic optical fiber gratings. *Biomed. Opt. Express* **2020**, *11*, 4862–4871. [CrossRef] [PubMed]
155. Udos, W.; Ooi, C.-W.; Tan, S.-H.; Lim, K.-S.; Ee, Y.J.; Ong, K.C.; Ahmad, H. Label-free surface-plasmon resonance fiber grating biosensor for Hand-foot-mouth disease (EV-A71) detection. *Optik* **2021**, *228*, 166221. [CrossRef]
156. Luo, B.; Xu, Y.; Wu, S.; Zhao, M.; Jiang, P.; Shi, S.; Zhang, Z.; Wang, Y.; Wang, L.; Liu, Y. A novel immunosensor based on excessively tilted fiber grating coated with gold nanospheres improves the detection limit of Newcastle disease virus. *Biosens. Bioelectron.* **2018**, *100*, 169–175. [CrossRef]
157. Lao, J.; Han, L.; Wu, Z.; Zhang, X.; Huang, Y.; Tang, Y.; Guo, T. Gold Nanoparticle-Functionalized Surface Plasmon Resonance Optical Fiber Biosensor: <italic>In Situ</italic> Detection of Thrombin With 1 n·M Detection Limit. *J. Lightwave Technol.* **2019**, *37*, 2748–2755. [CrossRef]
158. Luo, B.; Wang, Y.; Lu, H.; Wu, S.; Lu, Y.; Shi, S.; Li, L.; Jiang, S.; Zhao, M. Label-free and specific detection of soluble programmed death ligand-1 using a localized surface plasmon resonance biosensor based on excessively tilted fiber gratings. *Biomed. Opt. Express* **2019**, *10*, 5136–5148. [CrossRef]
159. Guo, T. Fiber Grating-Assisted Surface Plasmon Resonance for Biochemical and Electrochemical Sensing. *J. Lightwave Technol.* **2017**, *35*, 3323–3333. [CrossRef]
160. Sypabekova, M.; Korganbayev, S.; González-Vila, Á.; Caucheteur, C.; Shaimerdenova, M.; Ayupova, T.; Bekmurzayeva, A.; Vangelista, L.; Tosi, D. Functionalized etched tilted fiber Bragg grating aptasensor for label-free protein detection. *Biosens. Bioelectron.* **2019**, *146*, 111765. [CrossRef]
161. Guan, B.-O.; Li, J.; Jin, L.; Ran, Y. Fiber Bragg gratings in optical microfibers. *Opt. Fiber Technol.* **2013**, *19*, 793–801. [CrossRef]
162. Liu, T.; Liang, L.-L.; Xiao, P.; Sun, L.-P.; Huang, Y.-Y.; Ran, Y.; Jin, L.; Guan, B.-O. A label-free cardiac biomarker immunosensor based on phase-shifted microfiber Bragg grating. *Biosens. Bioelectron.* **2018**, *100*, 155–160. [CrossRef] [PubMed]
163. Ran, Y.; Long, J.; Xu, Z.; Yin, Y.; Hu, D.; Long, X.; Zhang, Y.; Liang, L.; Liang, H.; Guan, B.-O. Harmonic optical microfiber Bragg grating immunosensor for the accelerative test of cardiac biomarker (cTn-I). *Biosens. Bioelectron.* **2021**, *179*, 113081. [CrossRef] [PubMed]
164. James, S.W.; Tatam, R.P. Optical fibre long-period grating sensors: Characteristics and application. *Meas. Sci. Technol.* **2003**, *14*, R49–R61. [CrossRef]
165. Xuewen, S.; Lin, Z.; Bennion, I. Sensitivity characteristics of long-period fiber gratings. *J. Lightwave Technol.* **2002**, *20*, 255–266. [CrossRef]
166. DeLisa, M.P.; Zhang, Z.; Shiloach, M.; Pilevar, S.; Davis, C.C.; Sirkis, J.S.; Bentley, W.E. Evanescent Wave Long-Period Fiber Bragg Grating as an Immobilized Antibody Biosensor. *Anal. Chem.* **2000**, *72*, 2895–2900. [CrossRef] [PubMed]
167. Chiavaioli, F.; Trono, C.; Giannetti, A.; Brenci, M.; Baldini, F. Characterisation of a label-free biosensor based on long period grating. *J. Biophotonics* **2014**, *7*, 312–322. [CrossRef]
168. Dominik, M.; Leśniewski, A.; Janczuk, M.; Niedziółka-Jönsson, J.; Hołdyński, M.; Wachnicki, Ł.; Godlewski, M.; Bock, W.J.; Śmietana, M. Titanium oxide thin films obtained with physical and chemical vapour deposition methods for optical biosensing purposes. *Biosens. Bioelectron.* **2017**, *93*, 102–109. [CrossRef]
169. Quero, G.; Zuppolini, S.; Consales, M.; Diodato, L.; Vaiano, P.; Venturelli, A.; Santucci, M.; Spyrakis, F.; Costi, M.P.; Giordano, M.; et al. Long period fiber grating working in reflection mode as valuable biosensing platform for the detection of drug resistant bacteria. *Sens. Actuators B Chem.* **2016**, *230*, 510–520. [CrossRef]
170. Zuppolini, S.; Quero, G.; Consales, M.; Diodato, L.; Vaiano, P.; Venturelli, A.; Santucci, M.; Spyrakis, F.; Costi, M.P.; Giordano, M.; et al. Label-free fiber optic optrode for the detection of class C β-lactamases expressed by drug resistant bacteria. *Biomed. Opt. Express* **2017**, *8*, 5191–5205. [CrossRef]
171. Liu, C.; Xu, B.J.; Zhou, L.; Sun, Z.; Mao, H.J.; Zhao, J.L.; Zhang, L.; Chen, X. Graphene oxide functionalized long period fiber grating for highly sensitive hemoglobin detection. *Sens. Actuators B Chem.* **2018**, *261*, 91–96. [CrossRef]
172. Dong, J.; Sang, M.; Wang, S.; Xu, T.; Yu, X.; Liu, T. Ultrasensitive Label-Free Biosensor Based on the Graphene-Oxide-Coated-U-Bent Long-Period Fiber Grating Inscribed in a Two-Mode Fiber. *J. Lightwave Technol.* **2021**, *39*, 4013–4019. [CrossRef]
173. Wang, R.; Ren, Z.; Kong, D.; Hu, B.; He, Z. Highly sensitive label-free biosensor based on graphene-oxide functionalized micro-tapered long period fiber grating. *Opt. Mater.* **2020**, *109*, 110253. [CrossRef]
174. Cusano, A.; Iadicicco, A.; Pilla, P.; Contessa, L.; Campopiano, S.; Cutolo, A.; Giordano, M. Mode transition in high refractive index coated long period gratings. *Opt. Express* **2006**, *14*, 19–34. [CrossRef]
175. Pilla, P.; Manzillo, P.F.; Malachovska, V.; Buosciolo, A.; Campopiano, S.; Cutolo, A.; Ambrosio, L.; Giordano, M.; Cusano, A. Long period grating working in transition mode as promising technological platform for label-free biosensing. *Opt. Express* **2009**, *17*, 20039–20050. [CrossRef] [PubMed]
176. Chiavaioli, F.; Biswas, P.; Trono, C.; Jana, S.; Bandyopadhyay, S.; Basumallick, N.; Giannetti, A.; Tombelli, S.; Bera, S.; Mallick, A.; et al. Sol–Gel-Based Titania–Silica Thin Film Overlay for Long Period Fiber Grating-Based Biosensors. *Anal. Chem.* **2015**, *87*, 12024–12031. [CrossRef] [PubMed]

177. Esposito, F.; Sansone, L.; Taddei, C.; Campopiano, S.; Giordano, M.; Iadicicco, A. Ultrasensitive biosensor based on long period grating coated with polycarbonate-graphene oxide multilayer. *Sens. Actuators B Chem.* **2018**, *274*, 517–526. [CrossRef]
178. Esposito, F.; Sansone, L.; Srivastava, A.; Baldini, F.; Campopiano, S.; Chiavaioli, F.; Giordano, M.; Giannetti, A.; Iadicicco, A. Long period grating in double cladding fiber coated with graphene oxide as high-performance optical platform for biosensing. *Biosens. Bioelectron.* **2021**, *172*, 112747. [CrossRef]
179. Ramachandran, S.; Wang, Z.; Yan, M. Bandwidth control of long-period grating-based mode converters in few-mode fibers. *Opt. Lett.* **2002**, *27*, 698–700. [CrossRef]
180. Cheung, C.S.; Topliss, S.M.; James, S.W.; Tatam, R.P. Response of fiber-optic long-period gratings operating near the phase-matching turning point to the deposition of nanostructured coatings. *J. Opt. Soc. Am. B* **2008**, *25*, 897–902. [CrossRef]
181. Chen, X.; Zhou, K.; Zhang, L.; Bennion, I. Dual-peak long-period fiber gratings with enhanced refractive index sensitivity by finely tailored mode dispersion that uses the light cladding etching technique. *Appl. Opt.* **2007**, *46*, 451–455. [CrossRef]
182. Chiavaioli, F.; Biswas, P.; Trono, C.; Bandyopadhyay, S.; Giannetti, A.; Tombelli, S.; Basumallick, N.; Dasgupta, K.; Baldini, F. Towards sensitive label-free immunosensing by means of turn-around point long period fiber gratings. *Biosens. Bioelectron.* **2014**, *60*, 305–310. [CrossRef]
183. Liu, L.; Marques, L.; Correia, R.; Morgan, S.P.; Lee, S.-W.; Tighe, P.; Fairclough, L.; Korposh, S. Highly sensitive label-free antibody detection using a long period fibre grating sensor. *Sens. Actuators B Chem.* **2018**, *271*, 24–32. [CrossRef]
184. Dey, T.K.; Tombelli, S.; Biswas, P.; Giannetti, A.; Basumallick, N.; Baldini, F.; Bandyopadhyay, S.; Trono, C. Label-free immunosensing by long period fiber gratings at the lowest order cladding mode and near turn around point. *Opt. Laser Technol.* **2021**, *142*, 107194. [CrossRef]
185. Piestrzyńska, M.; Dominik, M.; Kosiel, K.; Janczuk-Richter, M.; Szot-Karpińska, K.; Brzozowska, E.; Shao, L.; Niedziółka-Jonsson, J.; Bock, W.J.; Śmietana, M. Ultrasensitive tantalum oxide nano-coated long-period gratings for detection of various biological targets. *Biosens. Bioelectron.* **2019**, *133*, 8–15. [CrossRef] [PubMed]
186. Lee, S.-L.; Kim, J.; Choi, S.; Han, J.; Seo, G.; Lee, Y.W. Fiber-optic label-free biosensor for SARS-CoV-2 spike protein detection using biofunctionalized long-period fiber grating. *Talanta* **2021**, *235*, 122801. [CrossRef]
187. Jeanmaire, D.L.; Van Duyne, R.P. Surface raman spectroelectrochemistry: Part I. Heterocyclic, aromatic, and aliphatic amines adsorbed on the anodized silver electrode. *J. Electroanal. Chem. Interfacial Electrochem.* **1977**, *84*, 1–20. [CrossRef]
188. Albrecht, M.G.; Creighton, J.A. Anomalously intense Raman spectra of pyridine at a silver electrode. *JACS* **1977**, *99*, 5215–5217. [CrossRef]
189. Moskovits, M. Surface-enhanced Raman spectroscopy: A brief retrospective. *J. Raman Spectrosc.* **2005**, *36*, 485–496. [CrossRef]
190. Ko, H.; Singamaneni, S.; Tsukruk, V.V. Nanostructured Surfaces and Assemblies as SERS Media. *Small* **2008**, *4*, 1576–1599. [CrossRef]
191. Marco, P.; Francesco, G.; Giorgio, G.; Giuseppe, Q.; Andrea, C. Self-assembled periodic patterns on the optical fiber tip by microsphere arrays. In Proceedings of the Volume 9634, 24th International Conference on Optical Fibre Sensors, Curitiba, Brazil, 28 September–2 October 2015; p. 96341N.
192. Managò, S.; Quero, G.; Zito, G.; Tullii, G.; Galeotti, F.; Pisco, M.; De Luca, A.C.; Cusano, A. Tailoring lab-on-fiber SERS optrodes towards biological targets of different sizes. *Sens. Actuators B Chem.* **2021**, *339*, 129321. [CrossRef]
193. Kim, J.A.; Wales, D.J.; Thompson, A.J.; Yang, G.-Z. Fiber-Optic SERS Probes Fabricated Using Two-Photon Polymerization For Rapid Detection of Bacteria. *Adv. Opt. Mater.* **2020**, *8*, 1901934. [CrossRef]
194. Yan, H.; Gu, C.; Yang, C.; Liu, J.; Jin, G.; Zhang, J.; Hou, L.; Yao, Y. Hollow core photonic crystal fiber surface-enhanced Raman probe. *Appl. Phys. Lett.* **2006**, *89*, 204101. [CrossRef]
195. Cox, F.M.; Argyros, A.; Large, M.C.J.; Kalluri, S. Surface enhanced Raman scattering in a hollow core microstructured optical fiber. *Opt. Express* **2007**, *15*, 13675–13681. [CrossRef] [PubMed]
196. Han, Y.; Koganemaru, M.; Ikeda, T.; Miyazaki, N.; Choi, W.; Tomokage, H. Impacts of uniaxial mechanical stress on high frequency performance of MOSFETs. In Proceedings of the 3rd Electronics System Integration Technology Conference ESTC, Berlin, Germany, 13–16 September 2010; pp. 1–5.
197. Zhang, Y.; Shi, C.; Gu, C.; Seballos, L.; Zhang, J.Z. Liquid core photonic crystal fiber sensor based on surface enhanced Raman scattering. *Appl. Phys. Lett.* **2007**, *90*, 193504. [CrossRef]
198. Dinish, U.S.; Fu, C.Y.; Soh, K.S.; Ramaswamy, B.; Kumar, A.; Olivo, M. Highly sensitive SERS detection of cancer proteins in low sample volume using hollow core photonic crystal fiber. *Biosens. Bioelectron.* **2012**, *33*, 293–298. [CrossRef]
199. Dinish, U.S.; Balasundaram, G.; Chang, Y.T.; Olivo, M. Sensitive multiplex detection of serological liver cancer biomarkers using SERS-active photonic crystal fiber probe. *J. Biophotonics* **2014**, *7*, 956–965. [CrossRef]
200. Hunter, R.; Sohi, A.N.; Khatoon, Z.; Berthiaume, V.R.; Alarcon, E.I.; Godin, M.; Anis, H. Optofluidic label-free SERS platform for rapid bacteria detection in serum. *Sens. Actuators B Chem.* **2019**, *300*, 126907. [CrossRef]
201. Dinish, U.S.; Beffara, F.; Humbert, G.; Auguste, J.-L.; Olivo, M. Surface-enhanced Raman scattering-active photonic crystal fiber probe: Towards next generation liquid biopsy sensor with ultra high sensitivity. *J. Biophotonics* **2019**, *12*, e201900027. [CrossRef]
202. Yang, X.; Gu, C.; Qian, F.; Li, Y.; Zhang, J.Z. Highly Sensitive Detection of Proteins and Bacteria in Aqueous Solution Using Surface-Enhanced Raman Scattering and Optical Fibers. *Anal. Chem.* **2011**, *83*, 5888–5894. [CrossRef]
203. Danny, C.G.; Subrahmanyam, A.; Sai, V.V.R. Development of plasmonic U-bent plastic optical fiber probes for surface enhanced Raman scattering based biosensing. *J. Raman Spectrosc.* **2018**, *49*, 1607–1616. [CrossRef]

204. Froggatt, M.; Moore, J. High-spatial-resolution distributed strain measurement in optical fiber with Rayleigh scatter. *Appl. Opt.* **1998**, *37*, 1735–1740. [CrossRef] [PubMed]
205. Sypabekova, M.; Aitkulov, A.; Blanc, W.; Tosi, D. Reflector-less nanoparticles doped optical fiber biosensor for the detection of proteins: Case thrombin. *Biosens. Bioelectron.* **2020**, *165*, 112365. [CrossRef] [PubMed]
206. Sypabekova, M.; Korganbayev, S.; Blanc, W.; Ayupova, T.; Bekmurzayeva, A.; Shaimerdenova, M.; Dukenbayev, K.; Molardi, C.; Tosi, D. Fiber optic refractive index sensors through spectral detection of Rayleigh backscattering in a chemically etched MgO-based nanoparticle-doped fiber. *Opt. Lett.* **2018**, *43*, 5945–5948. [CrossRef]
207. Ayupova, T.; Shaimerdenova, M.; Sypabekova, M.; Vangelista, L.; Tosi, D. Picomolar detection of thrombin with fiber-optic ball resonator sensor using optical backscatter reflectometry. *Optik* **2021**, *241*, 166969. [CrossRef]
208. Xu, X.; Chen, W.; Zhao, G.; Li, Y.; Lu, C.; Yang, L. Wireless whispering-gallery-mode sensor for thermal sensing and aerial mapping. *Light Sci. Appl.* **2018**, *7*, 62. [CrossRef] [PubMed]
209. Taitt, C.R.; Anderson, G.P.; Ligler, F.S. Evanescent wave fluorescence biosensors: Advances of the last decade. *Biosens. Bioelectron.* **2016**, *76*, 103–112. [CrossRef]
210. Epstein, J.R.; Walt, D.R. Fluorescence-based fibre optic arrays: A universal platform for sensing. *Chem. Soc. Rev.* **2003**, *32*, 203–214. [CrossRef] [PubMed]
211. Benito-Peña, E.; Valdés, M.G.; Glahn-Martínez, B.; Moreno-Bondi, M.C. Fluorescence based fiber optic and planar waveguide biosensors. A review. *Anal. Chim. Acta* **2016**, *943*, 17–40. [CrossRef] [PubMed]
212. Ahmad, M.; Hench, L.L. Effect of taper geometries and launch angle on evanescent wave penetration depth in optical fibers. *Biosens. Bioelectron.* **2005**, *20*, 1312–1319. [CrossRef]
213. Preejith, P.V.; Lim, C.S.; Chia, T.F. Serum protein measurement using a tapered fluorescent fibre-optic evanescent wave-based biosensor. *Meas. Sci. Technol.* **2006**, *17*, 3255–3260. [CrossRef]
214. Kapoor, R.; Wang, C.-W. Highly specific detection of interleukin-6 (IL-6) protein using combination tapered fiber-optic biosensor dip-probe. *Biosens. Bioelectron.* **2009**, *24*, 2696–2701. [CrossRef] [PubMed]
215. Saraswathi, P.; Shinoj, V.K.; Murukeshan Vadakke, M.; Parasuraman, P. Highly sensitive optical detection of specific protein in breast cancer cells using microstructured fiber in extremely low sample volume. *J. Biomed. Opt.* **2010**, *15*, 1–6. [CrossRef]
216. Hsieh, M.-C.; Chiu, Y.-H.; Lin, S.-F.; Chang, J.-Y.; Chang, C.-O.; Chiang, H.K. Amplification of the Signal Intensity of Fluorescence-Based Fiber-Optic Biosensors Using a Fabry-Perot Resonator Structure. *Sensors* **2015**, *15*, 3565–3574. [CrossRef]
217. Chang, Y.-F.; Chen, R.-C.; Lee, Y.-J.; Chao, S.-C.; Su, L.-C.; Li, Y.-C.; Chou, C. Localized surface plasmon coupled fluorescence fiber-optic biosensor for alpha-fetoprotein detection in human serum. *Biosens. Bioelectron.* **2009**, *24*, 1610–1614. [CrossRef]
218. Huang, J.C.; Chang, Y.-F.; Chen, K.-H.; Su, L.-C.; Lee, C.-W.; Chen, C.-C.; Chen, Y.-M.A.; Chou, C. Detection of severe acute respiratory syndrome (SARS) coronavirus nucleocapsid protein in human serum using a localized surface plasmon coupled fluorescence fiber-optic biosensor. *Biosens. Bioelectron.* **2009**, *25*, 320–325. [CrossRef]
219. Liu, G.; Zhang, K.; Nadort, A.; Hutchinson, M.R.; Goldys, E.M. Sensitive Cytokine Assay Based on Optical Fiber Allowing Localized and Spatially Resolved Detection of Interleukin-6. *ACS Sens.* **2017**, *2*, 218–226. [CrossRef] [PubMed]
220. Zhang, K.; Liu, G.; Goldys, E.M. Robust immunosensing system based on biotin-streptavidin coupling for spatially localized femtogram mL−1 level detection of interleukin-6. *Biosens. Bioelectron.* **2018**, *102*, 80–86. [CrossRef] [PubMed]
221. Chang, Y.-F.; Fu, C.; Chen, Y.-T.; Fang-Ju Jou, A.; Chen, C.-C.; Chou, C.; Annie Ho, J.-a. Use of liposomal amplifiers in total internal reflection fluorescence fiber-optic biosensors for protein detection. *Biosens. Bioelectron.* **2016**, *77*, 1201–1207. [CrossRef]
222. Presti, D.L.; Massaroni, C.; Leitão, C.S.J.; Domingues, M.D.F.; Sypabekova, M.; Barrera, D.; Floris, I.; Massari, L.; Oddo, C.M.; Sales, S.; et al. Fiber Bragg Gratings for Medical Applications and Future Challenges: A Review. *IEEE Access* **2020**, *8*, 156863–156888. [CrossRef]
223. Gao, R.; Lu, D.; Guo, D.; Xin, X. Dual-optofluidic waveguide in-line fiber biosensor for real-time label-free detection of interferon-gamma with temperature compensation. *Opt. Express* **2020**, *28*, 10491–10504. [CrossRef]
224. Wei, Y.; Zhou, W.; Wu, Y.; Zhu, H. High Sensitivity Label-Free Quantitative Method for Detecting Tumor Biomarkers in Human Serum by Optical Microfiber Couplers. *ACS Sens.* **2021**, *6*, 4304–4314. [CrossRef] [PubMed]
225. Delgado-Macuil, R.; González-León, K.; Beltrán-Pérez, G. Neuropsin (Opn5) detection in the brain tissue of a murine model using long period fiber grating (LPFG). *Opt. Laser Technol.* **2021**, *139*, 106972. [CrossRef]
226. Li, W.; Wang, H.; Yang, R.; Song, D.; Long, F.; Zhu, A. Integrated multichannel all-fiber optofluidic biosensing platform for sensitive and simultaneous detection of trace analytes. *Anal. Chim. Acta* **2018**, *1040*, 112–119. [CrossRef] [PubMed]
227. Wu, Q.; Qu, Y.; Liu, J.; Yuan, J.; Wan, S.P.; Wu, T.; He, X.D.; Liu, B.; Liu, D.; Ma, Y.; et al. Singlemode-Multimode-Singlemode Fiber Structures for Sensing Applications—A Review. *IEEE Sens. J.* **2021**, *21*, 12734–12751. [CrossRef]
228. Shaimerdenova, M.; Ayupova, T.; Sypabekova, M.; Tosi, D. Fiber Optic Refractive Index Sensors Based on a Ball Resonator and Optical Backscatter Interrogation. *Sensors* **2020**, *20*, 6199. [CrossRef] [PubMed]
229. Bekmurzayeva, A.; Ashikbayeva, Z.; Assylbekova, N.; Myrkhiyeva, Z.; Dauletova, A.; Ayupova, T.; Shaimerdenova, M.; Tosi, D. Ultra-wide, attomolar-level limit detection of CD44 biomarker with a silanized optical fiber biosensor. *Biosens. Bioelectron.* **2022**, *208*, 114217. [CrossRef]

230. Yang, X.; Luo, Y.; Liu, Y.; Gong, C.; Wang, Y.; Rao, Y.-J.; Peng, G.-D.; Gong, Y. Mass production of thin-walled hollow optical fibers enables disposable optofluidic laser immunosensors. *Lab A Chip* **2020**, *20*, 923–930. [CrossRef]
231. Li, C.; Liu, Y.; Lang, C.; Zhang, Y.; Qu, S. Femtosecond laser direct writing of a 3D microcantilever on the tip of an optical fiber sensor for on-chip optofluidic sensing. *Lab A Chip* **2022**, *22*, 3734–3743. [CrossRef]